Theory of structure and hyperfine properties of anomalous muonium in elemental semiconductors: Diamond, silicon, and germanium

N. Sahoo, S. B. Sulaiman, K. C. Mishra,* and T. P. Das
Department of Physics, State University of New York at Albany, Albany, New York 12222
(Received 19 September 1988; revised manuscript received 21 February 1989)

A number of possible models for the anomalous muonium (Mu*) center in the elemental semiconductors diamond, silicon, and germanium are investigated in detail, both with respect to their stabilities and abilities to explain the extensive available experimental hyperfine-interaction data, the latter being the major focus of the present work. Using the unrestricted Hartree-Fock cluster procedure, the electronic structures and potential-energy curves associated with muon positions are obtained for the different models. The results are utilized to obtain hyperfine properties associated with the muon and its neighboring nuclei, including vibrational effects associated with the muon. Our results show that stability considerations favor both the vacancy-associated (VA) and bond-centered (BC) models for Mu*. The VA model explains all the experimentally observed features of the muon hyperfine properties and provides reasonably good quantitative agreement with experiment. However, questions remain regarding its formation and ability to explain level-crossing resonance (LCR) data. On the other hand, although the BC model appears to explain the experimental features from LCR measurements, in its present form, it seriously overestimates the strengths of the muon hyperfine interactions as compared to experiment, by more than an order of magnitude in some cases. Additionally, it does not explain the trend from diamond through germanium. On the basis of the results in this paper for the VA and BC models, the direction for future investigations for understanding the nature of the Mu* center is commented on.

I. INTRODUCTION

Muonium is the bound state of a positively charged muon (μ^+) and an electron (e^-) and can be thought of as an ultralight isotope of hydrogen, the muon mass being only one-ninth of that of the proton. Two types of muonium centers are readily observed by muon-spin-rotation (μSR) experiments[1] when a positive muon is implanted in both elemental[2] and III-V compound[3] semiconductors. One of them is known[2,3] as the normal muonium center (Mu) and is characterized by its isotropic hyperfine interaction whose strength is a significant fraction of that of a free muonium. The other center is known[2,3] as anomalous muonium (Mu*) and has a rather anisotropic hyperfine interaction, with its strength very small as compared to both free muonium and Mu.

In both normal and anomalous muonium centers, the strength of the hyperfine interaction follows an irregular trend in going from diamond to germanium, namely a decrease from diamond to silicon and then an increase to germanium. The hyperfine parameters in both the centers have their largest values in diamond. In addition to this trend, the number of other features of the hyperfine interactions associated with the Mu* center have also been experimentally determined,[2,3] including superhyperfine interactions[4] with neighboring host nuclei in silicon and GaAs. These features are summarized in the next section.

The understanding of the nature and origin of these centers is of particular interest because they provide insights into the nature of hydrogen atoms trapped in semiconductors. Despite considerable effort, the exact locations of both the muonium centers have not yet been determined experimentally. However, various theoretical investigations[5] of the Mu center in elemental semiconductors have led to the consensus that it is a muonium trapped in the tetrahedral interstitial region.

In regard to the Mu* center, several possible models were proposed[6] in the literature prior to our quantitative analysis[7–11] of many such models and the proposition of the vacancy-associated (VA) model for Mu* in elemental semiconductors. We were led to the VA model through extensive investigations of the stability and hyperfine properties of a number of other models—namely, an excited muonium, a muonium in the hexagonal interstitial site, and a muonium at the center of the bond [bond-centered (BC) model]. It should be noted that in our earlier investigation[9,10] of the BC model we had not considered any relaxation of the host atoms adjacent to the muon. This is important in view of subsequent developments with the BC model which will be considered later in this section and in Secs. V and VI.

The results of our earlier analysis[7–11] showed that none of the other models[6] proposed for the Mu* have the capability of both leading to a stable energy minimum and explaining the observed features of the muon hyperfine data, while the VA model was successful on both counts. However, our investigations on the earlier models did suggest[9,10] that in the proper model for Mu*, the unpaired spin orbital should be comprised primarily of host-atom orbitals directed towards the muon with a relatively small spin density at the muon. Such a situation is well represented in the VA model where the muon

is located near a vacancy which provides a potential that leads to partial localization of the unpaired spin orbital down to the vicinity of the muon, leading to a small and anisotropic spin density at the muon site.

In our earlier communications,[8,10,11] we reported briefly how the VA model can successfully explain all the observed features of the muon hyperfine-interaction (hfi) tensor for Mu* in diamond, silicon, and germanium. Subsequent to our identification[8–11] of the VA model as a viable one for Mu*, it has been shown[12] that while the bond-centered model is unstable in a rigid lattice, it may become a stable site after allowing the atoms immediately adjacent to the muon to relax. Additionally, the results of level-crossing-resonance (LCR) measurements[4] have been successfully interpreted[4] using the BC model. This has led us to reexamine the bond-centered model in more detail for all three elemental semiconductors, especially with respect to hyperfine properties associated with the muon and superhyperfine interactions with neighboring host nuclei.

The aim of the present article is twofold. The first is to describe the results of our theoretical investigations on different possible models prior to our proposition[8] of the VA model and to present a systematic discussion of the features that they suggested to us for the appropriate model to have in order to explain the observed hyperfine properties[2] of the Mu* center. It is hoped that this discussion of the sequential process of arriving at an appropriate model for Mu* will not only permit useful insights into the nature of the Mu* center, but will also be helpful in providing some guidelines for a similar investigative search for other impurity centers in solid-state systems. The second aim is to make a critical assessment of the two competing models, VA and BC, that appear to be most in vogue at the present time, with the BC model supported by the results of LCR measurements. Our emphasis in this work is on critical examination of the abilities of the two models to explain both the many interesting qualitative features of the muon hyperfine data,[2] as well as the strengths of the observed hyperfine interactions in the three elemential semiconductors from a quantitative point of view.

This paper is organized in the following manner. Section II contains a brief review of the μSR and level crossing resonance data for Mu* in semiconductors. A brief description of the unrestricted Hartree-Fock cluster procedure used in our study of total-energy and hyperfine properties of Mu* is given in Sec. III. It was used for all the models studied, except the excited muonium model, which was treated semiquantitatively. In Sec. IV we analyze the VA model as well as other models[6] for Mu* that were proposed prior to the VA model. These include the excited-state model, the hexagonal-site model, and the rigid-bond-centered model. In Sec. V we describe the results of our investigations on the relaxed BC model. In Sec. VI a careful comparison is made between the VA model with the relaxed BC model, focusing especially on hyperfine properties. The impact of the results obtained in this work for the VA and BC models on directions for future investigations on the Mu* center is also remarked on in this section.

II. REVIEW OF μSR AND LCR EXPERIMENTAL RESULTS FOR Mu* IN SEMICONDUCTORS

A large body of data from various μSR experiments[2] on Mu* has been accumulated over the past few years and has been reviewed in the literature.[13] We will briefly describe here only the relevant results which will help us to decide between various possible models for Mu*.

The formation of muonium in semiconductors is observed[1] by the precession pattern of the muon spin under the influence of an applied magnetic field $\mathbf{B}$ and the hyperfine field due to the bound electron. The measured precession frequencies of Mu* could be described by a spin Hamiltonian

$$\mathcal{H}_{\mathrm{Mu}^*}=A_\perp(I_xS_x+I_yS_y)+A_\parallel I_zS_z-g_e\mu_B^e\mathbf{S}\cdot\mathbf{B}-g_\mu\mu_B^\mu\mathbf{I}\cdot\mathbf{B} \tag{1}$$

with its hyperfine-interaction tensor being axially symmetric about one of the four equivalent $\langle 111\rangle$ directions which is taken as the Z direction. In Eq. (1), $\mathbf{I}$ and $\mathbf{S}$ are spin operators of the muon and electron, respectively, and the last two terms describe the electron and muon Zeeman energies. $A_\parallel$ and $A_\perp$ correspond to the parallel and perpendicular components of hyperfine tensor $\overleftrightarrow{\mathbf{A}}$ with respect to the $\langle 111\rangle$ symmetry axis. These two components are related to the Fermi-contact and dipolar hyperfine coupling constants A and B by the relations $A_\parallel=A+2B$ and $A_\perp=A-B$. The experimental values[2] of the magnitudes of $A_\parallel$ and $A_\perp$ are given in Table I for the elemental semiconductors. The absolute signs of these components cannot be determined from experiment. However, from the magnetic field dependence of μSR frequencies,[13] the relative signs of $A_\parallel$ and $A_\perp$ are found to be negative for diamond and positive for silicon and germanium.

It has been found[14] that in diamond the normal-muonium signal disappears at high temperatures ($T>600$ K), whereas the Mu* signal can still be observed at these temperatures, suggesting a Mu-to-Mu* conversion at high temperatures. This conversion process is not very well observed[2,13] in Si and Ge, but it has been suggested[15] that the observed depolarization of Mu* in Si and Ge at temperatures near or above 150 and 75 K, respectively, may possibly be a result of Mu-to-Mu* conversion in these crystals. We are not concerned here about the origin of the conversion process, but one piece of information provided by Mu to Mu* conversion studies in a single crystal of diamond[16] is very useful for testing an appropriate model for Mu*. Thus, these studies have suggested that $A_\perp$ is negative for diamond, which makes $A_\parallel$ positive in view of the observed negative ratio[14] of $A_\parallel$ and $A_\perp$. If we also assume the same sign for $A_\perp$ in silicon and germanium, $A_\parallel$ has to be negative in these systems in view of the observed positive ratios[13] of $A_\parallel$ and $A_\perp$ in these systems. With these choices of absolute signs of $A_\parallel$ and $A_\perp$, one can obtain A and $2B$ for the three elemental semiconductors which are also listed in Table I.

Two site-sensitive experiments[17–19] have been reported in the literature for determining the location of muon in

TABLE I. Values of contact (A) and dipolar (B) contributions to muon hyperfine-interactions constants[a,b,c] for anomalous muonium in elemental semiconductors derived from experimental results for $A_{\parallel}$ and $A_{\perp}$.

Semiconductor	Observed sign of $A_{\parallel}/A_{\perp}$	$A_{\parallel}$	$A_{\perp}$	A	B
Diamond	−	±168.9	∓392.5	∓205.4	±186.1
Silicon	+	±16.8	±92.0	±66.9	±25.1
Germanium	+	±26.8	±130.7	±96.1	±34.6

[a]All numbers are in MHz.
[b]The magnitudes of $A_{\parallel}$ and $A_{\perp}$ are taken from Refs. 13 and 14.
[c]The two sets of signs for $A_{\parallel}$ and $A_{\perp}$ in the three systems are based on the observed signs of $A_{\parallel}/A_{\perp}$ combined with choices of positive and negative signs for $A_{\perp}$ (Refs. 13 and 14).

the Mu* state. One of them is the muon-decay channeling experiment[17] where the effect of blocking of the positrons from the muon decay was observed. The channeling data suggest[17] that muon occupies a site 0.9 Å away either from an occupied or vacant silicon ion position along the ⟨111⟩ axis. The other site-sensitive experiment[18,19] has utilized level-crossing-resonance spectroscopy, from which one can derive information about the hyperfine interaction of nuclei adjacent to the muon. Such information can, in principle, allow one to make inferences about the immediate environment of Mu*. The results of the LCR measurement in GaAs (Ref. 18) have predicted two distinct nuclear hyperfine parameters with axial symmetry around the ⟨111⟩ axis of the crystal. Also, the results of a very recent LCR experiment for Mu* in silicon[19] have been used to derive values of −137.5 and −73.96 MHz for the hyperfine parameters $A_{\parallel}^{n}$ and $A_{\perp}^{n}$ for a nearest-neighbor ^{29}Si atom located on the ⟨111⟩ axis. It has been suggested[18,19] that these LCR experimental data support a bond-centered location of Mu*. We shall discuss these experimental results further while comparing the predictions of our theoretical hyperfine-interaction results for both the BC and VA models in Sec. VI.

The effect of electron irradiation on the Mu* signal has also been investigated experimentally[20] in the literature. The main motivation behind these experiments was to learn about the interaction between the muonium and defects such as vacancies and interstitials which are produced by the irradiation process. The following observations[13,20] are made from these studies. It is found that electron irradiation of silicon tends to enhance the Mu* signal and, in strongly doped materials, the Mu* signal can only be observed after the irradiation. However, preformed vacancies do not increase the initial Mu* amplitude in electron-irradiated samples. The Mu-to-Mu* transition, however, is promoted by radiation-induced defects. The possible implications of these observations for the VA and BC models will be discussed in Sec. VI.

In concluding this section, it can be said that the hyperfine properties of Mu* are very accurately known from experiment. Other observed features such as the nature of the Mu to Mu* transition, the site determination of muon in Mu* and its interaction with defects are not yet as definitive and need more experimental effort before a consensus on them can be reached. Thus, any successful model for Mu* in elemental semiconductors should at least account for the following observed features of $\overleftrightarrow{A}$: (a) the small values of its components, (b) its oblateness, (c) the irregular trend in its strength in going from diamond to germanium, (d) the opposite sign of its components $A_{\parallel}$ and $A_{\perp}$ in diamond and same sign for both in Si and Ge, and (e) the negative sign for $A_{\perp}$ in diamond. These are the properties which we feel are the most conclusively known and we have focused on them in attempting to decide on the proper model for Mu*. The other features including the superhyperfine data from LCR measurements can be used as auxiliary tests of the competing models.

III. UHF-LCAO-MO CLUSTER PROCEDURE AND PROCEDURE FOR EVALUATION OF HYPERFINE PROPERTIES

The molecular-cluster procedure,[21] using a small number of atoms representing an explicit region of solid in real space, has proved to be very satisfactory in studying the structures and properties of a variety of systems, such as ionic crystals,[22] point defects in semiconductors[23] and insulators,[24] and chemisorption at semiconductor surfaces.[25] It is a particularly useful procedure in investigating the location and hyperfine structure of impurity atoms both in the bulk[23] and surfaces[25] of semiconductors. This is because the perturbation produced by the impurity atom in the strong covalent bonds in these materials is expected to be localized to a small region around the impurity and thus the use of a finite-size cluster is not expected to be a very serious limitation. In this procedure one chooses as large a cluster involving the impurity and its surroundings as is practicable from a computational point of view, being careful, of course, about the expected symmetry of the center. To simulate the effect of the rest of the semiconducting solid outside of the cluster, the dangling bonds at the surface of the cluster are saturated with hydrogen atoms[26] since the electronegativity of hydrogen is close to that of the elemental semiconductors. Thus, in the cluster procedure, the imperfect solid is approximated as a large molecule, which allows one to apply first-principles methods like the unrestricted Hartree-Fock self-consistent procedure[27] used in the present work, to study the electronic structure of Mu* in semiconductors. One can test the sensitivity of the ener-

gy and other properties to the size of the cluster by examining the effect of including more host atoms in the cluster. Our choice of saturator hydrogen–host-atom bond distance will be described while discussing the clusters employed in our calculation.

The details of the variational unrestricted Hartree-Fock (UHF) procedure that we have used here are available in the literature.[27] We shall present only a brief description here both for the sake of completeness and because it is necessary for our discussions later in this paper. In the UHF procedure it is assumed, as in standard self-consistent one-electron procedures, that each electron moves in the average field of the other electrons. The antisymmetrized wave function Ψ of the many-electron system is represented by a single Slater determinant composed of the occupied molecular orbitals ψ_μ. In Roothaan's linear combination of atomic orbitals–molecular orbitals (LCAO-MO) approach,[28] each molecular orbital ψ_μ is expanded as

$$\psi_\mu = \sum_i c_{\mu i}\phi_i \ , \tag{2}$$

where the ϕ_i are one-electron atomic orbitals. The molecular-orbital coefficients $c_{\mu i}$ are treated as variational parameters which are obtained through iterative solution of a set of linear equations known as Hartree-Fock-Roothaan equations. The space part of the one-electron atomic orbitals in the present work are constructed using a linear combination of Cartesian Gaussian functions[29] of the form

$$\chi_i = N_{in} x_n^{a_i} y_n^{b_i} z_n^{c_i} e^{-\zeta r_n^2} \ , \tag{3}$$

with $a_i+b_i+c_i=l_i$, l_i referring to the angular momentum of the orbital involved. In the above expression, N_{in} is the normalization factor, and x_n, y_n, z_n, and r_n are the coordinates and distance referred to the nucleus n about which the basis orbital i is considered to be centered. The use of Gaussian orbitals permits analytic evaluation of the one-electron and two-electron integrals occurring in the calculation, which allows substantial savings in computational time. Further, as is customary in the UHF approximation,[27] the spatial parts of the spin-up and spin-down molecular-orbital pairs are taken to be different. This allows the incorporation of spin-polarization effects in a first-principles manner.

A knowledge of the potential-energy curve for the impurity atom in the solid is needed for studying both the location of and vibrational effects associated with the impurity atom. The latter is particularly important for a light impurity like the muon. The potential-energy curve can be obtained by studying the variation of the total energy of the cluster considered with the position of the impurity atom. The position for which the potential energy is minimum corresponds to the equilibrium site of the muon inside the solid. The procedure for studying vibrational effects will be discussed later in this section.

Turning next to the evaluation of hyperfine properties, the magnetic hyperfine tensor for the Mu* center is known to be axially symmetric.[13] In such a case, one needs to calculate the Fermi-contact and dipolar hyperfine constants[30] A and B in MHz, which, in terms of the UHF wave functions, are given by the following two equations:[30]

$$A(\mathbf{R}) = \tfrac{4}{3}\gamma_e\gamma_N\hbar(10^{-6}a_0^{-3})\left[\sum_v [\,|\psi_{v\uparrow}(\mathbf{R})|^2 - |\psi_{v\downarrow}(\mathbf{R})|^2] + |\psi_{u\uparrow}(\mathbf{R})|^2\right] , \tag{4}$$

$$B(\mathbf{R}) = \frac{\gamma_e\gamma_N\hbar}{4\pi}(10^{-6}a_0^{-3})\left[\sum_v (\langle\psi_{v\uparrow}|\hat{O}|\psi_{v\uparrow}\rangle - \langle\psi_{v\downarrow}|\hat{O}|\psi_{v\downarrow}\rangle) + \langle\psi_{u\uparrow}|\hat{O}|\psi_{u\uparrow}\rangle\right] ,$$

v referring to the paired spin orbitals and u to the unpaired spin orbitals. The position vector of the nucleus N where the hyperfine constants are calculated is given by $\mathbf{R}$, and $\hat{O}$ is the dipole operator $[(3\cos^2\theta-1)/(r^3)]$, γ_e and γ_n being the magnetogyric ratios for the electron and the nucleus N. The components $A_\parallel$ and $A_\perp$ of the axially symmetric hyperfine tensor $\overleftrightarrow{\mathbf{A}}$ can be obtained from A and B using the relations

$$A_\parallel = A+2B, \quad A_\perp = A-B \ . \tag{5}$$

The oblateness of the observed Mu* hyperfine tensor,[13,14] which corresponds to $|A_\parallel| < |A_\perp|$, thus requires A and B to have opposite signs, making the spin-polarized nature of the UHF procedure rather important, since it allows A to be negative, which is not possible for the restricted Hartree-Fock procedure in which paired spin orbitals with opposite spin are assumed to have the same spatial wave function.

In most of our UHF calculations, we have used the STO-3G (Ref. 31) approximation for the atomic orbitals ϕ_i in the molecular orbital expansion in Eq. (1) (STO denotes Slater-type orbital, G Gaussian). Each atomic orbital is expressed as a linear combination of three Cartesian Gaussians in the form

$$\phi_i = \sum_{j=1}^{3} d_{ij}\chi_j \ , \tag{6}$$

the coefficients d_{ij} being obtained by making a least-squares fit to the corresponding Slater-type atomic orbitals. In some situations, to allow for better variational flexibility, we have also used a set of split-valence basis functions available in the literature such as 3-21G,[32] which consists of two contracted Gaussians and one uncontracted Gaussian. Since a number of cluster calculations, each involving a large number of atoms, are attempted in this work, it was not possible to use a more extensive set of basis functions, because this would have required an inordinately large amount of computer time. However, the choice of minimal STO-3G and 3-21G basis sets have been found to be quite suitable from numerous calculations[31–33] of equilibrium geometry and electronic structures of small molecules and clusters. The UHF calculations were carried out using the GAUSSIAN-80 (Ref.

34) and GAUSSIAN-86 (Ref. 35) systems of programs.

Lastly, since the muon is a rather light particle, it was necessary to average the hyperfine constants over the vibrational wave functions associated with the motion of the muon in the lattice. The vibrationally averaged hyperfine constants $\langle A \rangle$ (and $\langle B \rangle$) can be obtained using the relation

$$\langle A \rangle = \int |\psi_v(\mathbf{R})|^2 A(\mathbf{R}) d^3R \ . \quad (7)$$

The three-dimensional average can often be expressed in terms of one-dimensional averages from either symmetry considerations[36] or the nature of the potential experienced by the muon in the lattice and the variation of $A(\mathbf{R})$ with the direction of R. The vibrational functions $\psi_v(\mathbf{R})$ in Eq. (7) have been obtained variationally using the calculated potential for the muon in the lattice. Hermite polynomials were used for the basis functions employed in the variational procedure. More details of this vibrational averaging procedure will be discussed in Secs. IV and V dealing with our results for the VA and BC models for Mu*.

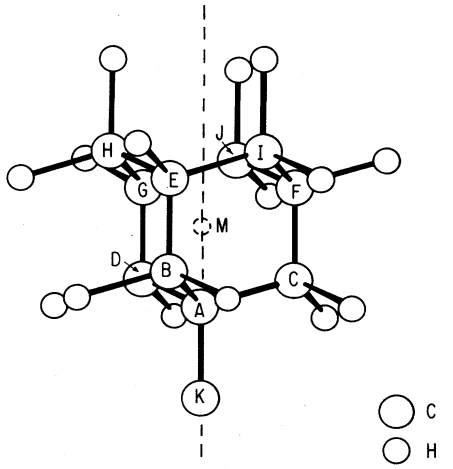

FIG. 1. Twenty-seven–atom cluster, $C_{10}H_{16}(\mu^+e^-)$, used for investigation of the hexagonal-site model for Mu*. The muon is represented by the symbol M and is allowed to move along and perpendicular to the $\langle 111 \rangle$ axis shown by the dashed line, both within the hexagonal region spanned by the atoms E–J and outside.

IV. VACANCY-ASSOCIATED MODEL AND PRIOR MODELS

In this section we shall discuss in the detail the VA model. Before we discuss this model, however, it is useful to briefly describe other models that were proposed prior to the VA model and how their analysis led us to the VA model.

A. Excited-state model

The very first model suggested for Mu* in the literature[37] in elemental semiconductors was an excited state of Mu located in the tetrahedral interstitial region of the diamond lattice, at a site of C_{3v} symmetry away from the interstitial with T_d symmetry. At a C_{3v} site the degenerate excited $2s$ and $2p$ states of Mu are expected to mix with each other, leading to an axially symmetric hyperfine field at the muon. The contact and dipolar fields at the muon site due to the $2s$ and $2p_z$ orbitals in free muonium are

$$A_{2s} = 558 \text{ MHz}, \quad B_{2p_z} = 28 \text{ MHz} \ , \quad (8)$$

respectively. These values are small compared to $A_{1s} = 4463$ MHz, which was the rationale for the proposition of the excited-state model. However, the value of B_{2p_z} appears to be much too small compared to the values of B (Table I) needed to explain the experimental values[13,14] of $A_{\parallel}$ and $A_{\perp}$, suggesting that one would need substantially larger than 100% $2p_z$ character in diamond and about 90% in silicon, the latter being also rather implausible to expect in the interstitial site. This expectation has been borne out from earlier[38] semiempirical self-consistent-charge extended Hückel (SCCEH) cluster calculations[39] for Mu* in silicon with the muon located at a distance[40] of 1.6 Å away from the tetrahedral interstitial site towards the silicon atom A in Fig. 1. This calculation not only showed rather weak admixture of $2s$ and $2p$ states, leading to a relatively small value of B, but also that A and B have the same sign, which would lead to a prolate hyperfine tensor, in disagreement with experiment.[13,14] Both this consideration, as well as the fact that in the excited-state model Mu* would be unstable with respect to Mu, in contrast to the observation[14] of greater stability of Mu* with respect to Mu in diamond at higher temperatures, and an expected similar feature in silicon and germanium, rule out the excited-state model.

Although this model did not appear to be the likely one, the investigations on it did provide valuable insight into some of the requirements for a plausible model for Mu*. Thus, the local contribution from the $2p$ orbital is, by itself, rather inadequate to explain the observed[13,14] dipolar field term B (Table I) and one needs a model where there is a substantial dipolar contribution from the tails of the host-atom orbitals. Secondly, to explain the oblate character of the hyperfine tensor, Eqs. (5) suggest that for a positive B, one needs a negative A. A negative value of A can be obtained only when one includes exchange-polarization effects[41] arising from the paired spin orbitals which can be done using the UHF procedure which has been used in the analysis of all the subsequent models discussed in this article.

B. Analysis of the hexagonal-site model

The next model we have examined is the hexagonal-site model proposed in the literature[37] and we examined it because of its threefold symmetry, which is in keeping with the observed axial symmetry of the muon hyperfine tensor. A neutral muonium center at the hexagonal site was, however, found to be unrepresentative of the Mu* center, both because our earlier work on the normal muonium center in diamond[7,42] and silicon[43] led to a maximum at the hexagonal site instead of a minimum, and also be-

cause of the very large spin density at the muon leading to a contact hyperfine field an order of magnitude higher than observed.

The center we have explored for the hexagonal-site model is one involving a doubly charged environment. The reasons for choosing this environment were the following. First, the very large hyperfine interaction for the neutral environment was the result of the electron around the muon in a $1s$-like state. An environment with the $1s$ electron missing was therefore tried, a doubly charged situation being used to get an odd number of electrons and hence an unpaired spin. This choice for the hexagonal-site model with the unpaired electron not on the muonium, but primarily on the host atoms, also allowed a test of the expectation in the preceding subsection that the host orbitals could make a stronger contribution than the muonium $2p$ orbital needed to explain the observed anisotropic muon hyperfine constant for Mu*. A charged muonium center could be produced by ionization of electrons from host atoms by the muon along its pathway in the crystal.

For our investigation of the hexagonal-site center that we carried out in diamond, we employed a 27-atom cluster, which, in addition to the μ^+e^- complex, involves the 10 carbon atoms $A-J$ in Fig. 1 and 16 hydrogen atoms to saturate the dangling bonds on the carbon atoms. The saturator hydrogen atoms were placed at a distance of 1.54 Å from the carbon atoms in the cluster, corresponding to the C—C bond length in diamond. This choice is considered[44] to be an appropriate one for studying interstitial impurities because it provides both the correct average band gap[45] in diamond and charge neutrality for the atoms when one uses a 26-atom cluster of the type described above, without the μ^+e^- complex, to simulate pure diamond. The STO-3G minimal basis set[31] was used for the carbon $1s,2s,2p$ and hydrogen and muonium orbitals. The potential-energy curve (PEC) (Ref. 7) for the muon obtained by our UHF cluster investigation exhibited two minima—one at the hexagonal site and a much shallower one 0.4 Å away from the tetrahedral interstitial site, 1.14 Å from atom A in Fig. 1, indicating that the hexagonal site was the trapping site. To test the stability of our result with respect to cluster size, we also studied a smaller cluster involving the μ^+e^- complex and six carbon atoms $E-J$ with saturator hydrogen atoms for the dangling bonds, again obtaining the minimum at the hexagonal site. The hyperfine constants obtained with the smaller and larger clusters were, respectively, ($A=-10.5$ MHz, $B=32.0$ MHz) and ($A=-3.5$ MHz, $B=35.0$ MHz). The similarity of these two results, along with the fact that they are not too different quantitatively, indicate that the result for the larger cluster is representative of the actual situation for the hexagonal center.

The smallness of the values of A and B obtained for the hexagonal model compared to the values $A=-205$ MHz and $B=186.9$ MHz from the experimental[14] $A_\parallel$ and $A_\perp$ indicates that this model could be ruled out for Mu*. This conclusion is also in keeping with the result of a recent channeling experiment.[17] However, the analysis of the charged interstitial hexagonal model provided useful insights into the features needed for the proper model for Mu* to explain the observed muon hyperfine interaction. Thus, the value of B for this model being larger than the value of 28 MHz for the localized $2p$ muonium orbital, justifies the expectation from a consideration[38] of the excited-state model that molecular orbitals involving primarily host orbitals are needed to explain the observed Mu* hyperfine data. However, the relative smallness of the value of B for this model suggests that the molecular orbitals associated with the host atoms for the Mu* center should have more directed character than this model. These considerations led us to explore the rigid-bond-centered model to be discussed next.

C. Rigid-bond-centered model

In keeping with the criterion of having more directed host atom orbitals in the molecular wave functions, the rigid-bond-centered model for the Mu* has the μ^+e^- complex located at the center of a bond[46] between two host atoms strongly overlapping the orbitals for the latter. For our investigations on this model,[9,10] both a small cluster, ($C_2H_6\mu^+e^-$), and a larger one, ($C_8H_{18}\mu^+e^-$), were tried in order to study the convergence of our results with respect to cluster sizes. The small cluster [Fig. 2(a)] involved the two carbon atoms, nearest neighbors of the muon with separation of 1.545 Å corresponding to the host diamond crystal. The dangling

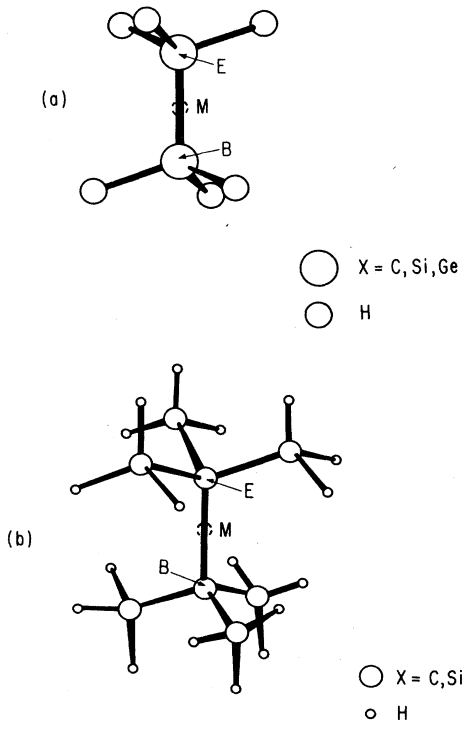

FIG. 2. Clusters used to simulate the BC model for elemental semiconductors. The position of the muon is represented by M and is varied both along and perpendicular to the bond along the ⟨111⟩ axis. (a) represents the smaller 9-atom cluster $X_2H_6(\mu^+e^-)$ (X=C, Si, Ge), and (b) the large 27-atom $X_8H_{18}(\mu^+e^-)$ (X=C, Si) cluster.

bonds on these carbon atoms were saturated with hydrogens with the C-H distance equal to 1.091 Å as in CH_4; this choice was preferred over that for the hexagonal interstitial model because the environment now is more molecular in nature in contrast to the weak perturbation over the host crystal in the former case. The larger cluster [Fig. 2(b)] included the second-nearest-neighbor carbon atoms and their saturator hydrogen atoms. STO-3G basis functions[31] were also employed for all the atoms in both the clusters.

Potential-energy curves, as a function of muon position, were studied for this model for both the direction of the C—C bond and that perpendicular to it. These curves showed very little variation for the two different sized clusters indicating good convergence. While the PEC along the C—C bond showed a minimum at the center, that perpendicular to it showed a maximum indicating instability of this center without any lattice relaxation. Additionally, the hyperfine constants A and B for the muon at the bond center were found to be -661 and 727 MHz, respectively, much larger than the values needed in Table I to explain the observed[13,14] $A_{\parallel}$ and $A_{\perp}$. We have also studied, in our earlier calculation, the nature of the PEC's for a small expansion in the length of the C—C bond on which the muon was located and had observed a flattening of the maximum in the perpendicular direction. However, the value of A increased, further accentuating the difference with experiments.[13,14] Subsequently, the BC model has been further examined in the literature[47–52] for both Mu* and hydrogen and found to show a minimum in the PEC for both along and perpendicular to C—C direction when very sizable expansion is made in the C—C distance. We shall discuss this model[53] in detail in the next subsection. In the rest of the subsection we will discuss the results we have obtained with the VA model which we were led to by our analysis of the three earlier models discussed in this section.

D. Vacancy-associated model

The results of our investigations on the different possible models described in the last three sections suggested that in the appropriate model for Mu*, the unpaired electron should be in a delocalized orbital comprised mainly of host atomic orbitals directed towards the muon with a relatively small spin density at the muon site. The rest of the spin density would be expected to be distributed on the host atoms. This situation is well represented in a vacancy-associated model we have proposed earlier.[8–10] The presence of the vacancy leads to four dangling bonds which can be directed towards the muon, the spin density at the muon arising primarily from the tails of these dangling bonds, thus producing the required small values of the muon hyperfine parameters.

An important question that has to be decided upon in analyzing the VA model is the choice of the charge and symmetry of the vacancy-associated environment of Mu*. Of the five charge states, $V^{2\pm}$, $V^{1\pm}$, V^0, known[54] to exist for vacancies in semiconductors, only when the μ^+e^- system is trapped near the $V^{2\pm}$ and V^0 sites can one obtain an odd number of electrons and explain the paramagnetic nature of the Mu* center. Out of these three choices, a consideration of the observed axial symmetry of the hyperfine tensor and possible Jahn-Teller distortion[55] leads to the conclusion that V^{2+} is the only appropriate choice for the Mu* center. This can be understood from an examination of Fig. 3 where we present the energy level schemes for different charge states for the pure vacancy and vacancy-muonium composite systems with the muon located at a site adjacent to the vacancy.

Figure 3(a) presents the energy levels expected from the combination of four sp^3 hybrid dangling bonds associated with V^0. Since such a center has tetrahedral (T_d) point-group symmetry, this combination leads to a state belonging to the A_1 representation of the T_d symmetry group and another belonging to the triply degenerate T_2 representation. From a number of earlier investigations,[56] it has been found that the A_1 state has a lower energy and thus gets filled by two of the four electrons belonging to the four dangling bonds, the other two electrons occupying the T_2 state. Such a partially filled electronic state is unstable under Jahn-Teller distortion and the symmetry of the center would be lowered to C_{2v} point-group symmetry to remove this degeneracy. A similar situation occurs when the muonium (μ^+e^-) gets trapped near the V^0 site along the $\langle 111 \rangle$ direction, the level structure and electronic population for which are presented in Fig. 3(b). In this case, the symmetry of the center is C_{3v} and the T_2 state of the previous case splits into a nondegenerate A_1 state and a doubly degenerate E state. Additionally, there is one more A_1 state which is associated with the interaction between the muonium $1s$ orbital and the dangling bond orbitals and is found from our cluster calculations to occur at a much higher energy than the E state and the other two A_1 states. The five electrons available, four from the dangling bonds associated with the vacancy and one from the muonium will be distributed over the energy levels in the manner shown in Fig. 3(b). This situation will again be Jahn-Teller unstable because of the partially filled twofold degenerate E level. As shown in Fig. 3(c), the symmetry would then be expected to be lowered to that of C_{2v} and the E-like state will split into nondegenerate B_1 and B_2 states. Such a

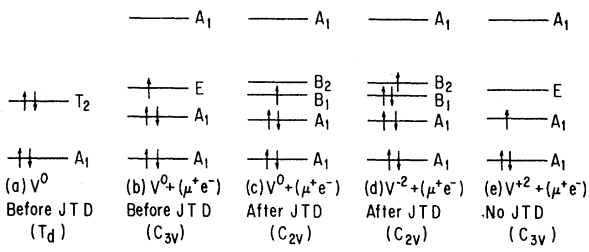

FIG. 3. Energy-level diagrams (schematic) for neutral vacancy V^0 and for μ^+e^- trapped near V^0 and $V^{2\pm}$. JTD represents Jahn-Teller distortion. The symmetries of the various centers are noted in the figure. The level orderings for μ^+e^- located near V^0 and $V^{2\pm}$ sites are obtained from UHF cluster calculations.

center would therefore not be able to explain the experimentally observed[13,14] axially symmetric hyperfine tensor. In the case of a μ^+e^- complex located along the $\langle 111 \rangle$ direction near a negatively charged vacancy V^{2-}, an analogous situation occurs as shown in Fig. 3(d). In this case, one again has C_{2v} symmetry after Jahn-Teller distortion. There are two additional electrons as compared to the V^0 associated center, one of which occupies the B_1 state leading to complete pairing of this state and the other occupies the B_2 state. Again, from the symmetry of the B_2 state where the unpaired electron resides, one cannot explain the observed axial symmetry of the hyperfine tensor. For the case of a μ^+e^- complex trapped near a positively charged vacancy, V^{2+}, the energy-level diagram in Fig. 3(e), leads one to expect that Jahn-Teller effect will not occur because the unpaired electron is in a nondegenerate A_1 state. This state has the right symmetry for explaining the observed axially symmetric $\overleftrightarrow{\mathbf{A}}$ tensor. This environment thus seems to be the appropriate one for the vacancy-associated center.

We have applied the same UHF cluster procedure described in Sec. III to study the potential energy and electronic structure of the μ^+e^- complex located in the V^{2+} environment. The clusters of atoms used in our investigations[8-10] can be described using Fig. 4. The first cluster ($X_4H_{12}\mu^+e^-$) used for all three semiconductors, diamond, silicon, and germanium, involves 17 atoms, composed of the μ^+e^- system and four host atoms *B*, *C*, *D*, and *E* (denoted as *X*) surrounding the vacancy at *A* with each of the host atoms saturated by three hydrogen atoms, located at the *X-H* covalent bond distance for reasons discussed in Sec. IV C. The STO-3G (Ref. 31) basis function was used for the atomic orbitals of all the atoms included in the cluster. First we studied the variation of the total energies for the cluster with muon positions along $\langle 111 \rangle$ direction on both sides of the vacancy *A*, in Fig. 4, in all the three systems. These total energies are plotted in Figs. 5–7 for diamond, silicon, and germanium, respectively, these curves representing the PEC's governing the vibrational motions of the muon. In all cases, there are two minima in the PEC's on either side of the vacancy *A*. The positions of the minima in the PEC's on the right in Figs. 5–7 (corresponding to displacement of the muonium towards the atom *E* in Fig. 4 along the $\langle 111 \rangle$ axis) are close to the C—H, Si—H, and Ge—H covalent bond distances from *E*, while those on the left correspond to having the muon located at a position whose distance from the *BCD* plane (Fig. 4) is about 70% of that from the vacancy *A* to the *BCD* plane.

For diamond, the larger depth of the minimum on the left as compared to that on the right (Fig. 5) indicates that the combined strength of the bonding between the muon and the three atoms *B*, *C*, and *D* dominates over that associated with the single bond it would form with the atom *E* if it was located at the right-hand minimum. For silicon and germanium, the reverse appears to be true, with the minimum on the right being the deeper one. We have also studied the variation of energy with muon motion along a perpendicular direction to $\langle 111 \rangle$ in the neighborhood of the two minima and found an increase in the total energy, establishing the fact that the two minima in Figs. 5–7 are absolute ones.

We also studied the effect of cluster size on the potential energy for muon motion and on the electronic structure of the VA center using two larger clusters for diamond and silicon, one associated with muon position above the vacancy towards the plane formed by the three host atoms *BCD* and the other one for muon positions below the vacancy in the direction of atom *E*. In the latter case, a 27-atom cluster ($X_{10}H_{18}\mu^+e^-$, X=C,Si) was used which included the second-nearest-neighbor host atoms *I*–*N* in Fig. 4 in addition to *B*–*E*. Similarly for the former case, we used 26 atoms which included host atoms *B*–*H*, corresponding to a cluster ($X_8H_{17}\mu^+e^-$, X=C,Si). These two clusters with C_{3v} symmetry were chosen with the aim of trying to include all the second nearest neighbors of muon in its displaced positions with respect to the vacancy. The inclusion of

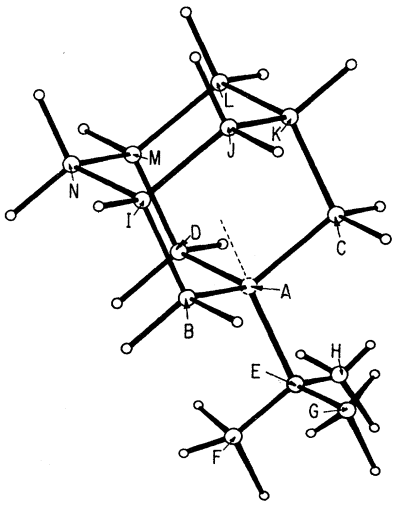

FIG. 4. Atomic environment associated with VA model for Mu*. The vacancy is at *A* and the muon is located on the $\langle 111 \rangle$ axis shown by dotted lines.

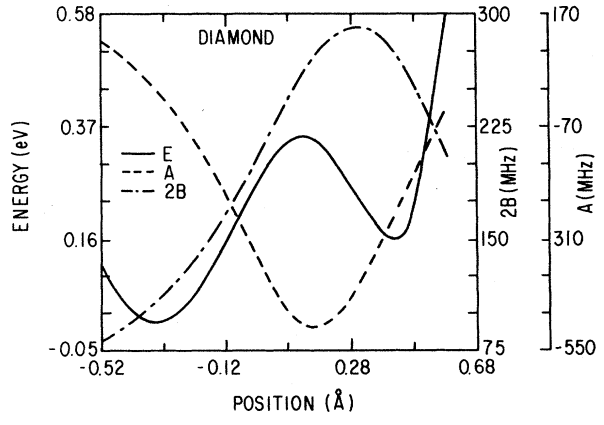

FIG. 5. Potential-energy curve and curves representing variations of muon hyperfine constants *A* and 2*B* with muon hyperfine constants *A* and 2*B* with muon positions along $\langle 111 \rangle$ axis for the VA model in diamond.

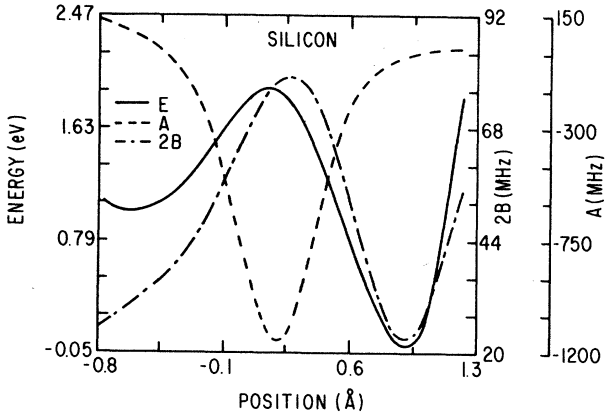

FIG. 6. Potential-energy curve and curves representing variations of muon hyperfine constants A and $2B$ with muon hyperfine constants A and $2B$ with muon positions along $\langle 111 \rangle$ axis for the VA model in silicon.

all the nearest-neighbor host atoms of the atoms *BCDE* would have led to a prohibitively large cluster from a computational point of view. These two large clusters chosen for diamond and silicon would be impracticable to use for all-electron calculations for germanium which involves many more orbitals and electrons per host atom. The positions and natures of the minima for diamond and silicon were unchanged with respect to those in Figs. 5–7 on using these larger clusters, indicating that the smaller cluster results are quite representative of environment of the muon in the real solid-state system. Thus, the trapping of the μ^+e^- system near a V^{2+} site is well supported from energy considerations. The stability of this vacancy-associated system can be understood physically as resulting from the extra attraction provided by the interaction of the positive charge of V^{2+} with the electron of μ^+e^- system. That this center corresponds to Mu* will now be demonstrated by analyzing its hyperfine properties using the calculated electronic wave functions and averaging them over the variational motion of the muon in the potentials represented by the energy curves in Figs. 5–7.

The contact and dipolar hyperfine constants A and $2B$ obtained using Eqs. (4) together with the electronic wave functions for the $(X_4H_{12}\mu^+e^-)$ cluster are also plotted in

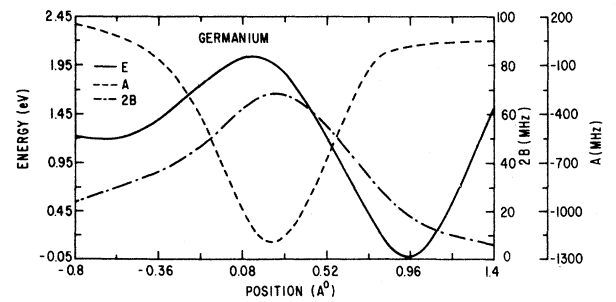

FIG. 7. Potential-energy curve and curves representing variations of muon hyperfine constants A and $2B$ with muon hyperfine constants A and $2B$ with muon positions along $\langle 111 \rangle$ axis for the VA model in germanium.

Figs. 5–7 as a function of muon positions for diamond, silicon, and germanium. The contact term A is seen to be negative in most of the region covered in these figures, indicating the dominance of the exchange-polarization contribution in Eqs. (4) over the direct term. The dipolar hyperfine constant B is seen to be positive everywhere, the condition for an oblate A being thus satisfied over most of the region where the muon is trapped.

In view of the strong variations in the PEC as well as A and $2B$ (Figs. 5–7) for the VA model with the position of the muon for all three systems, it is necessary to carry out a vibrational averaging of A and $2B$ in making comparisons with experiment. In principle, one should carry out a three-dimensional vibrational averaging. However, for the present model, a one-dimensional averaging in the $\langle 111 \rangle$ direction was considered adequate because both A and $2B$ were found to be quite insensitive to small displacements perpendicular to $\langle 111 \rangle$ axis. However, for the relaxed BC model to be discussed in the next section, a three-dimensional averaging is necessary and we will consider this more general procedure now so that this discussion will be appropriate for both models.

For three-dimensional averaging, the vibrational wave function needed should ideally be obtained as a function of the vector $\mathbf{R}$ describing the motion of the muon in three dimensions. This is, however, rather time consuming to do from a computational point of view. We have instead assumed the vibrational motions in the three directions corresponding to $\langle 111 \rangle$ and the two directions perpendicular to it to be independent of each other. This is a reasonable approximation in view of the reflection symmetries associated with both the VA model and the relaxed BC model. Representing the components of the displacement of the muon with respect to a chosen origin of the $\langle 111 \rangle$ axis as $\mathbf{R}_{\mu z}$ (parallel to the $\langle 111 \rangle$ direction), $\mathbf{R}_{\mu x}$ and $\mathbf{R}_{\mu y}$ (along two directions mutually perpendicular to $\langle 111 \rangle$), symmetry considerations lead to the absence of cross terms containing odd powers of $\mathbf{R}_{\mu x}$, $\mathbf{R}_{\mu y}$, and $\mathbf{R}_{\mu z}$ in the potential energy for muon motion. Thus cross terms like $R_{\mu x}R_{\mu y}$, $R_{\mu x}^3R_{\mu y}$, and $R_{\mu x}R_{\mu y}^3$ will be absent in the lowest-order bilinear and the next nonvanishing higher-order quartic terms in the potential energy. The only quartic cross terms present would be those like $R_{\mu x}^2R_{\mu y}^2$ and unless their amplitudes are significant, which we have found not to be the case in the present work, one can neglect these terms. This makes the independent averaging procedure for the three directions X, Y, and Z a justifiable one. With this assumption, the vibrational average $\langle A \rangle$ of Fermi contact term A can be written as

$$\langle A \rangle = \int \psi_v^2(R_{\mu z})\psi_v^2(R_{\mu x})\psi_v^2(R_{\mu y}) \times [A_0 + \Delta A_z(R_{\mu z}) + \Delta A_x(R_{\mu x}) + \Delta A_y(R_{\mu y})]dR_{\mu z}\,dR_{\mu x}\,dR_{\mu y} . \quad (9)$$

The functions $\psi_v(R_{\mu z})$, $\psi_v(R_{\mu x})$, and $\psi_v(R_{\mu y})$ represent the vibrational wave functions for the x, y, and z directions. The quantity A_0 is the value of A at the origin, while $\Delta A_z(R_{\mu z})$, $\Delta A_x(R_{\mu x})$, and $\Delta A_y(R_{\mu y})$ represent the variations in A with displacements in the three direc-

tions. This is again a reasonable approximation from symmetry considerations when the displacements with respect to origin are not too large. Using Eq. (9) and the axial symmetry about the ⟨111⟩ axis, one can write

$$\langle A \rangle = \langle A \rangle_z + 2\langle A \rangle_x - 2A_0 , \tag{10}$$

where

$$\langle A \rangle_z = \int \psi_v^2(R_{\mu z}) A(R_{\mu z}) dR_{\mu z}$$

and

$$\langle A \rangle_x = \int \psi_v^2(R_{\mu x}) A(R_{\mu x}) dR_{\mu x} . \tag{11}$$

The corresponding relations also hold for $\langle B \rangle$, namely,

$$\langle B \rangle = \langle B \rangle_z + 2\langle B \rangle_x - 2B_0 , \tag{12}$$

where

$$\langle B \rangle_z = \int \psi_v^2(R_{\mu z}) B(R_{\mu z}) dR_{\mu z}$$

and

$$\langle B \rangle_x = \int \psi_v^2(R_{\mu x}) B(R_{\mu x}) dR_{\mu x} . \tag{13}$$

The vibrational wave functions $\psi_v(R_{\mu z})$ and $\psi_v(R_{\mu x})$ are eigenfunctions of the Hamiltonians $\mathcal{H}(R_{\mu z})$ and $\mathcal{H}(R_{\mu x})$ for muon vibrations given by

$$\mathcal{H}(R_{\mu z}) = -\frac{\hbar^2}{2m}\frac{\partial^2}{\partial R_{\mu z}^2} + V(R_{\mu z}) \tag{14}$$

and

$$\mathcal{H}(R_{\mu x}) = -\frac{\hbar^2}{2m}\frac{\partial^2}{\partial R_{\mu x}^2} + V(R_{\mu x}) , \tag{15}$$

where the potentials $V(R_{\mu z})$ and $V(R_{\mu x})$ are given by the calculated PEC's for the Z and X directions. The function $\psi_v(R_{\mu z})$ was determined variationally using the expansion

$$\psi_v(R_{\mu z}) = \sum_n C_n \Phi_n(R_{\mu z}) , \tag{16}$$

where the $\Phi_n(R_{\mu z})$ are basis functions corresponding to eigenfunctions of a harmonic-oscillator potential fitted to the appropriate PEC for the ⟨111⟩ direction. The summation in n was taken over the ground and 19 excited vibrational states in the harmonic-oscillator potential. The vibrational function which is needed for the relaxed BC model discussed in the next section was obtained by a similar procedure using the PEC perpendicular to the ⟨111⟩ direction.

For vibrational averaging of A and $2B$ for the VA model, as remarked earlier, a one-dimensional treatment involving the ⟨111⟩ direction is considered to be adequate. The ground-state vibrational wave functions $\psi_v(R_{\mu z})$ were obtained variationally using the potential curves in Figs 5–7 where $R_{\mu z}$ was measured from the vacancy site. These wave functions indicated complete localization of the muon in the deeper potential wells in Figs. 6 and 7 for silicon and germanium while in the case of diamond there was a small but significant penetration into the shallower potential well.

The vibrationally averaged results $\langle A \rangle$ and $\langle 2B \rangle$ that we have obtained for the VA model for the three systems are tabulated in Table II, together with the parameters $\langle A_\parallel \rangle$ and $\langle A_\perp \rangle$ evaluated using Eqs. (5). The measured[13,14] values of the magnitudes of these quantities and relative signs from experiment are also listed for ready comparison.

It can be seen from Table II that the results for $\langle A_\parallel \rangle$ and $\langle A_\perp \rangle$ for the VA model are in agreement with all the observed features of the experimental results[13,14] for the muon hyperfine parameters in Mu*. Thus, both $\langle A_\parallel \rangle$ and $\langle A_\perp \rangle$ satisfy the trend of decrease in magnitude in going from diamond to silicon and increase from silicon to germanium with the germanium values smaller than in diamond. Secondly, the relative signs of $A_\parallel$ and $A_\perp$ are found to agree with experiment in all three cases. Thirdly, the absolute sign of $A_\perp$ which has been obtained experimentally[16] is in agreement with the theoretical prediction from the VA model. In regards to absolute magnitudes, there is reasonably good agreement with experiment for silicon and germanium, the results for diamond being smaller than experiment by factors of 3.1 for $A_\parallel$ and 2.5 for $A_\perp$, respectively. One likely source for improvement in agreement with experiment for the absolute magnitudes within the framework of the Hartree-Fock cluster theory is the inclusion of lattice relaxation effects which will entail, for its satisfactory treatment, the use of larger clusters than have been employed here. Inclusion of many-body effects could also help in bridging the gap between theory and experiment. These will require an order of magnitude larger amount of computational effort than what has been needed in obtaining the present results.

We have also evaluated the superhyperfine-interaction parameters for the nearest- and next-nearest-neighbor host ^{13}C, ^{29}Si, and ^{73}Ge nuclei adjacent to the muon. In case of diamond, there are three equivalent nearest-neighbor nuclei associated with the host atoms B, C, and D in Fig. 4 while E represents the next-nearest neighbor.

TABLE II. Vibrationally averaged muon hyperfine parameters in MHz for Mu* for the vacancy-associated model for diamond, silicon, and germanium compared with experiment.

	Theoretical				Experimental[a]		
Semiconductor	$\langle A \rangle$	$\langle 2B \rangle$	$\langle A_\parallel \rangle$	$\langle A_\perp \rangle$	$\lvert A_\parallel \rvert$	$\lvert A_\perp \rvert$	Sign of $A_\parallel / A_\perp$
Diamond	−85.0	139.0	54.0	−155.0	167.9	392.5	−
Silicon	−55.0	32.0	−25.0	−71.0	16.8	92.6	+
Germanium	−70.0	25.0	−45.0	−82.0	26.8	130.7	+

[a]Taken from Refs. 13 and 14.

The reverse situation applies to silicon and germanium. Our results for the superhyperfine parameters of these two groups of nuclei after averaging over the one-dimensional vibration of muon along the ⟨111⟩ axis are tabulated in Table III. The superhyperfine tensor for the nucleus at E is axially symmetric and therefore one needs only the isotropic parameter A and the dipolar parameter B corresponding to the ⟨111⟩ axis which is chosen as the Z axis. For the other three nuclei at the B, C, and D sites, the symmetry is not axial. We have therefore evaluated the principal components of the dipolar tensor B which are listed in Table III. The cosines of angles of orientation $\gamma_{ii'}$, of these principal axes ($i'=x'$, y', and z') for the nucleus at B with respect to the original axes ($i=x$, y, and z) for diamond are

$$\gamma_{ii'}=\begin{bmatrix} 0.000 & 1.000 & 0.000 \\ 0.497 & 0.000 & -0.868 \\ 0.868 & 0.000 & 0.497 \end{bmatrix}, \tag{17}$$

for silicon,

$$\gamma_{ii'}=\begin{bmatrix} 0.000 & 1.000 & 0.000 \\ -0.945 & 0.000 & 0.328 \\ 0.328 & 0.000 & 0.945 \end{bmatrix}, \tag{18}$$

and for germanium,

$$\gamma_{ii'}=\begin{bmatrix} 0.000 & 1.000 & 0.000 \\ -0.941 & 0.000 & 0.338 \\ 0.338 & 0.000 & 0.941 \end{bmatrix}. \tag{19}$$

The principal axes for the equivalent nuclei at C and D can be obtained by appropriate rotations. It is hoped that these predictions for the superhyperfine interactions can be tested with measurements using enriched nuclei in the future.

Before passing on to a description of our results on the relaxed BC model, it is appropriate to point out a few experimental results that provide some support for the occurrence of the VA model for Mu*. Thus, the measurement of the blocking effect on channeling of positron[17] from muon decay has suggested vacancy as a possible trapping site for Mu*. The infrared measurement[57] of hydrogen stretching frequencies suggests evidence of hydrogen (muonium) trapping near vacancies. A vacancy-hydrogen complex has also been identified[58] in proton bombarded silicon by deep-level transient spectroscopy (DLTS) measurements. This complex was found to disappear below room temperature as has been found[13] for Mu* in silicon and germanium. There are also significant correlations[13] between the vacancy annealing temperatures and the temperatures at which Mu* disappears in silicon and germanium. The disappearance of Mu* in silicon and germanium above 165 and 85 K, respectively, could be attributed to the observed instability of vacancies between 130 and 180 K in silicon[59] and at 65 K in germanium.[60] Also, the observation of Mu* at very high temperatures in diamond[14] may be due to the stability of vacancies up to 700 K in this material.[61] Another source of support for the VA model is the observation[3] of similarities between the Mu* hyperfine parameters in GaP and GaAs. This has led to the suggestion[3] that Mu* may be associated with the P and As vacancies in GaP and GaAs, respectively. Thus, the Ga atom being the immediate neighbors in both cases, one can expect the same hyperfine structure for both systems.

TABLE III. Calculated superhyperfine-interaction parameters in MHz for Mu* in diamond, silicon, and germanium for the vacancy-associated model. (a) For the nucleus located on the ⟨111⟩ axis (nucleus E of Fig. 14) which is the next nearest neighbor of muon in diamond and nearest neighbor of muon in silicon and germanium. (b) For the three equivalent nuclei located off the ⟨111⟩ axis (nuclei B, C, and D of Fig. 14) which are nearest neighbors of muon in diamond and next nearest neighbors of muon in silicon and germanium.

(a)

Semiconductor	A	B
Diamond	695.0	85.7
Silicon	−39.3	−9.3
Germanium	−7.9	−2.0

(b)

Semiconductor	A	B_{xx}	B_{yy}	B_{zz}
Diamond	43.5	−5.7	−5.0	10.7
Silicon	−167.9	−63.4	29.5	33.9
Germanium	−35.0	−15.6	7.2	8.4

V. RELAXED-BOND-CENTERED MODEL

We shall now consider the muon hyperfine properties of the relaxed-bond-centered model for Mu*, which has received strong support from the analysis of recent LCR measurements.[4] The model which includes relaxation of host atoms has been investigated[47–50] in the literature using the cluster approach. Two of these investigations[47,48] have utilized the UHF procedure and limited relaxation involving displacements of only the two nearest neighbors of the muon. The other investigations[49,50] have utilized an approximation to the UHF procedure referred to as PRDDO (partial retention of diatomic differential overlap) which allowed them to include displacements of the next-nearest neighbors of the muon.

The recent UHF investigation[47] on diamond including lattice relaxation effects has shown that the maximum found at the bond-centered site for displacements of the muon perpendicular to the ⟨111⟩ axis becomes a minimum for substantial displacements of the nearest-neighbor carbon atoms from the equilibrium positions, as was expected by the results of our earlier investigation[9,10] where only relatively small displacements of the carbon atoms were examined. Thus, for about 40% relaxation of the carbon atoms from their equilibrium positions, one obtains an absolute energy minimum[47] at the bond center in diamond, indicating that this could be a plausible location for the muon. For this lattice relaxation, the distance between each carbon and the muonium was 1.07 Å, very close to the average C—H bond distance in organic molecules. For silicon,[48] UHF investigations have shown

that the stable position of muon on the Si—Si bond was not at the bond center but closer to one of the silicons at a bond distance of 1.44 Å, close to the Si—H bond length and significantly further from the other silicon atom. The expansion of the Si—Si bond length is again about 40 percent compared to the perfect crystal. The investigations by the PRDDO method in diamond,[49] like the UHF investigation[47] in this material, considered only symmetric relaxation of the nearest- and next-nearest-neighbor carbon atoms. An absolute minimum was found in the PEC for muon at the bond-centered site when the C—C bond distance was expanded by about 42%, close to the result from the UHF investigation. A similar investigation has also been reported[50] for silicon by the PRDDO procedure. The minimum in PEC was again found at the center of the Si—Si bond after the bond distance was expanded by about 34% of that in pure crystalline silicon. This is in contrast to the asymmetric position found in the UHF investigation.[48] It should also be mentioned here that two recent investigations[51,52] aimed at studying the location of hydrogen in silicon have also demonstrated that there is a minimum in the bond-centered region. However, one of them,[51] utilizing a supercell procedure based on a pseudopotential approach and local density approximation has obtained an energy minimum at the bond center as in the PRDDO cluster calculation[50] on the Mu* center. The other one,[52] using an MNDO (modified neglect of different overlap) cluster procedure has obtained a minimum away from the bond center as in the UHF cluster investigation[48] on Mu*.

In view of the very large displacements of the nearest-neighbor host atoms in the BC model, one would, of course, like to test the nature of the minimum in the PEC using the first-principle UHF procedure allowing a very sizable number of host atom neighbors beyond the first and second nearest ones to relax. However, the results obtained so far[47–52] do provide evidence that there is a trapping site for the muon on the host atom bond in the ⟨111⟩ direction when one allows for a very sizable displacement of the nearest-neighbor atoms from their equilibrium positions. The situation regarding whether the muon is on the bond center or off it seems to be unclear, but all these investigations suggest that the muon is located at a position which is close to the C—H or Si—H bond distance away from the nearest host atom. The crucial question, of course, is whether this trapping site does in fact correspond to the Mu* center.

For this model or, for that matter, any other model to be identified with the Mu* center, it is very important that it be able to explain the features of the substantial amount of muon hyperfine data that have accumulated for the Mu* center.[13,14] These features have been discussed in Sec. II and involve not only the oblate symmetry of the hyperfine tensor and the magnitudes of its components, but also the irregular trend in the latter for the series, diamond, silicon, and germanium, the relative signs of $A_{\parallel}$ and $A_{\perp}$, and the absolute signs in diamond. Our recent investigations[53] on the relaxed BC model for diamond, silicon, and germanium, which will now be described, have focused on the question of the validity of this model for Mu* from the point of view of hyperfine properties. The earlier investigations[47–50] on the relaxed BC model for Mu* have calculated only the contact contribution to the hyperfine field, which, similar to our earlier result[9,10] in the unrelaxed lattice, comes out substantially larger (a factor of 3 to 4) compared to experiment.[13,14]

We have carried out hyperfine structure investigations for the relaxed BC model for all three elemental semiconductors diamond, silicon, and germanium including lattice relaxation effects. Our investigations have included a study of the hyperfine properties of both the symmetric and asymmetric locations of muon found in the recent cluster investigations.[47–50] Considering first the case of diamond, we have studied two clusters of different sizes namely, $C_2H_6\mu^+e^-$ shown in Fig. 2(a) and $C_8H_{18}\mu^+e^-$ in Fig. 2(b) to examine the sensitiveness of hyperfine properties to the cluster sizes. This was important for our investigations on silicon and germanium where the use of the large cluster is rather time consuming. The two clusters studied for diamond have the same topologies as the rigid-lattice clusters used in our earlier work.[9,10] The difference now is that the host atoms are displaced from their positions in the perfect crystal by an amount found in the recent cluster calculations.[47,49] In Fig. 2(a) the C—C bond distance was expanded by 42% in keeping with the results of the recent PRDDO calculation[49] involving a larger cluster. However, this bond distance is close to that found in the Hartree-Fock calculation[47] which used a smaller cluster. The saturator hydrogens were located at a distance of 1.091 Å (the usual C—H bond distance in organic molecules) away from the undisplaced positions of the carbon atom in the perfect lattice. With this choice, the C(1)C(2)H bond angle for the displaced positions of the carbon atoms is found to be close to the corresponding angle obtained from the PRDDO calculation.[49] The ratio between the C(1)—H bond distances in the unrelaxed and relaxed clusters with this choice is also very close to the ratio of the distance between C(1) and its nearest-neighbor carbon atoms [other than C(2)] in the unrelaxed and relaxed positions found in the PRDDO calculation.[49] This observation was very useful in choosing the geometry of the clusters we have employed for silicon and germanium. Additionally, as we have remarked earlier, the C(1)—μ^+ and C(2)—μ^+ bond distances in the relaxed lattice are very close[47,49] to the normal C—H bond distances in organic molecules. For the bigger cluster shown in Fig. 2(b), the positions of the nearest-neighbor carbon atoms of C(1) and C(2) were taken from the PRDDO investigation,[47] these atoms being saturated with hydrogen atoms with the C-H distances equal to the usual value of 1.091 Å. This choice is justified, by the arguments in Sec. IV C, because the corresponding C—C bond distance in the relaxed lattice was found[49] to be 1.55 Å, close to the value of 1.545 Å for the perfect diamond crystal.

In regards to the basis functions employed in our investigations, we have used 3-21G split valence Gaussian basis functions[32] both for carbon and the muonium. A minimal basis function consisting of three contracted

Gaussians[62] was utilized for the saturator hydrogen atom.

With these choices of 9- and 27-atom clusters [Figs. 2(a) and 2(b)] and basis set, we have studied the PEC's and contact and dipolar hyperfine interactions at the muon as a function of muon position with respect to the bond center in directions parallel and perpendicular to the C(1)—C(2) direction. The PEC's were studied for two reasons. The first reason was to verify that one indeed obtained minima in the PEC's at the bond center for the chosen clusters in both the directions parallel and perpendicular to C(1)—C(2) in Figs. 2(a) and 2(b). The second reason was to use the calculated PEC's to carry out vibrational averaging of hyperfine properties. The PEC's for the two directions are shown in Figs. 8 and 9 for both the small and large clusters used in our calculation. They are both seen to exhibit minima at the bond center. However, while the PEC is seen to vary rather steeply along the bond direction, C(1)—C(2) as one gets away from the bond center, in the perpendicular direction the variation is rather flat. Thus, vibrational averaging effects would be more pronounced for the perpendicular direction because of the expected larger extension of the vibrational wave functions in this case. Additionally, the PEC's for the 9- and 27-atom clusters are seen to be quite close to each other for both directions indicating rapid convergence with respect to cluster size.

The Fermi contact and dipolar hyperfine constants A and $2B$ for the muon obtained using Eqs. (4) are plotted in Figs. 10–13 as a function of the muon position (R_μ) with respect to the bond center for the 9- and 27-atom clusters and for both the $\langle 111 \rangle$ direction and the direction perpendicular to it. These curves are seen to have the following features. First, A is seen to be negative in most of the region around the minimum in the PEC while $2B$ is seen to be positive in this region. This feature would be expected from Eqs. (5) to explain the oblate nature of the hyperfine tensor, namely $|A_\parallel| < |A_\perp|$. Secondly, the curves $A(R_\mu)$ and $2B(R_\mu)$ are seen to vary rather rapidly in the $\langle 111 \rangle$ direction, Thus, even though the PEC is rather steep about the minimum position for this direction, one still expects vibrational effects to be quite important. For the perpendicular direction, as

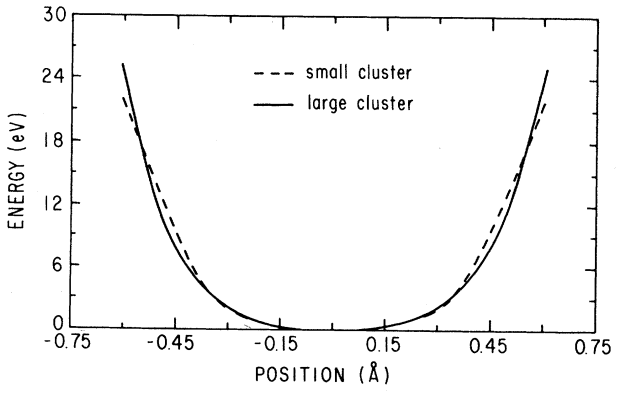

FIG. 8. Potential-energy curves for muon along the $\langle 111 \rangle$ axis for the BC model for the small and large clusters in diamond.

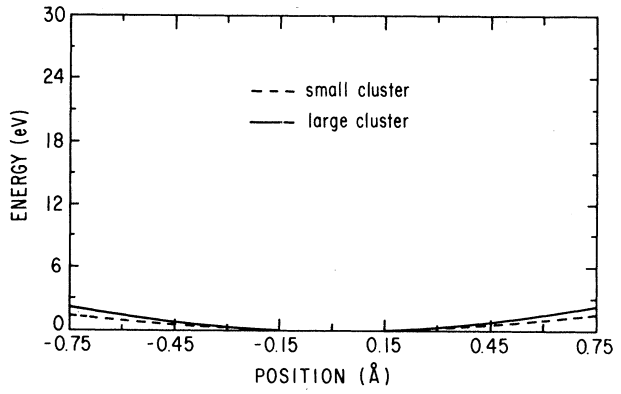

FIG. 9. Potential-energy curves for muon along the direction perpendicular to the $\langle 111 \rangle$ axis for the BC model for the small and large clusters in diamond.

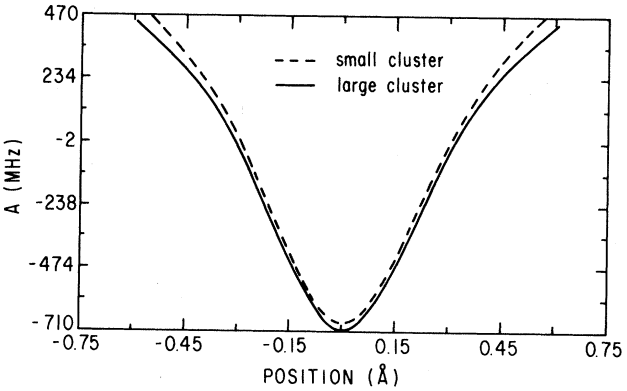

FIG. 10. Variation of the Fermi contact hyperfine constant A for muon with its position along $\langle 111 \rangle$ axis for the BC model for the small and large clusters in diamond.

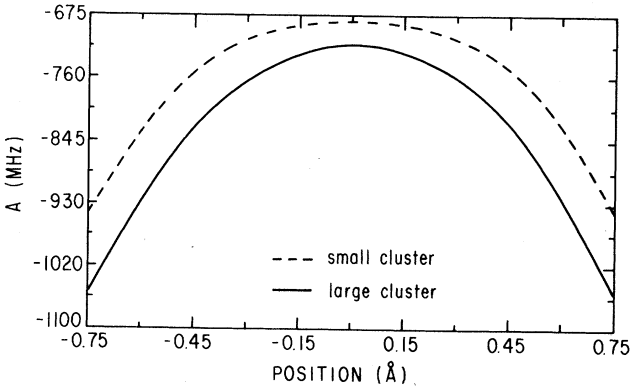

FIG. 11. Variation of the Fermi contact hyperfine constant A for muon with its position along the direction perpendicular to the $\langle 111 \rangle$ axis for the BC model for the small and large clusters in diamond.

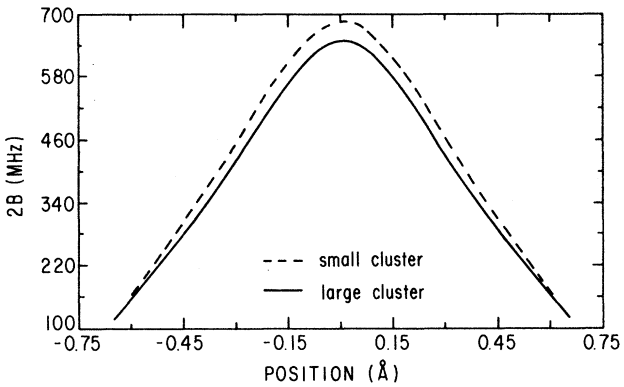

FIG. 12. Variation of the dipolar hyperfine constant $2B$ for muon with its position along $\langle 111 \rangle$ axis for the BC model for the small and large clusters in diamond.

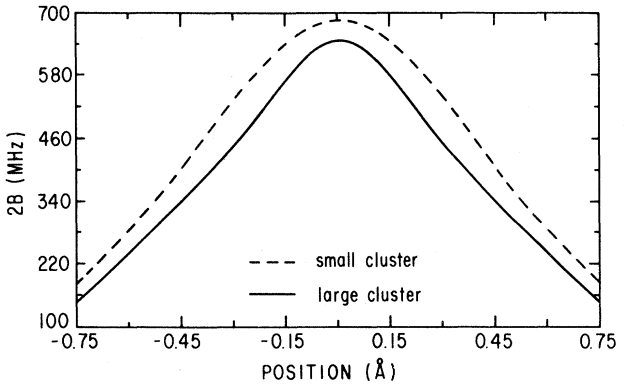

FIG. 13. Variation of the dipolar hyperfine constant $2B$ for muon with its position along the direction perpendicular to the $\langle 111 \rangle$ axis for the BC model for the small and large clusters in diamond.

remarked earlier, the flatness of the PEC makes the vibrational averaging important in this direction as well.

The procedure for carrying out averaging of the contact and dipolar hyperfine parameters A and $2B$ for vibrational motions along and perpendicular to the $\langle 111 \rangle$ axis has been already described in Sec. IV D. The expressions for the averages of A and $2B$ are given in Eqs. (10)–(13) and the procedure for determining the vibrational wave functions for the motions in the $\langle 111 \rangle$ direction and perpendicular to it using the corresponding PEC's are also described in Sec. IV D. Since the PEC's for the 9- and 27-atom clusters were quite close to each other, one does not expect any significant difference when one uses either of these curves for vibrational averaging. An important feature of our results was that the admixtures of excited vibrational states to the ground states in Eq. (16) for the $\psi_v(R_{vz})$ were rather small, indicating that the PEC for the relaxed BC model fitted a harmonic-oscillator potential rather well. A similar observation was found to apply for the $\psi_v(R_{\mu x})$. Using these vibrational functions, $\langle A \rangle_z$, $\langle A \rangle_x$, $\langle B \rangle_z$, and $\langle B \rangle_x$ in Eqs. (11) and (13) were obtained by carrying out the integrations occurring in these equations.

The theoretical values for the hyperfine constants for the relaxed BC model for Mu* in diamond are listed in Table IV. Under each entry, the first row refers to the 9-atom cluster and the second row to the 27-atom cluster. The entries under the bond-centered value refer to the values of A and $2B$ obtained from Eqs. (4) at the center of the C—C bond in Figs. 2(a) and 2(b). The vibrational averages along the $\langle 111 \rangle$ and perpendicular directions are obtained using Eqs. (11) and (13) utilizing the corresponding curves for A and $2B$ as a function of muon position in Figs. 10–13 and the PEC's in Figs. 8 and 9. The

TABLE IV. Calculated values of muon hyperfine constants A, $2B$, $A_{\parallel}$, and $A_{\perp}$ in MHz for anomalous muonium in diamond for the bond-centered model.

	Cluster	A	$2B$	$A_{\parallel}$	$A_{\perp}$
Bond-centered value	Small	−681.5	689.2	7.7	−1026.1
	Big	−712.2	652.9	−59.2	−1038.6
Average along $\langle 111 \rangle$	Small	−534.3	644.6	110.2	−856.6
	Big	−548.9	605.5	56.5	−851.7
Average along $\langle 111 \rangle_{\perp}$[a]	Small	−693.1	624.1	−69.1	−1005.1
	Big	−730.9	549.0	−181.9	−1005.4
Net-average value	Small	−557.6	514.2	−43.4	−814.7
	Big	−586.3	510.6	−75.8	−841.6
Experimental value		−205.4	374.3	168.9	−392.5

[a]$\langle 111 \rangle_{\perp}$ denotes direction perpendicular to $\langle 111 \rangle$.

[b]Experimentally (Refs. 13 and 14) the ratio of $A_{\parallel}$ and $A_{\perp}$ is known to be negative and $A_{\perp}$ is also negative (Ref. 16) for diamond.

entries under net average for A and $2B$ refer to the values obtained using Eqs. (10) and (12). The values of $A_{\parallel}$ and $A_{\perp}$ in Table IV for the various cases are obtained from the corresponding values of A and B using Eqs. (5). The experimental values of $A_{\parallel}$ and $A_{\perp}$ and A and $2B$ are also included in Table IV for ready reference. The sign of the experimental value of $A_{\perp}$ is taken as negative from Ref. 16. The sign of $A_{\parallel}$ has then to be positive to make the ratio of $A_{\parallel}/A_{\perp}$ negative as observed experimentally.[13,14] The experimental values of A and $2B$ in Table IV are obtained from the values of $A_{\parallel}$ and $A_{\perp}$ using Eqs. (5).

From Table IV it appears that the results for small and large clusters are very close when considering vibrational motion for the large and small clusters along $\langle 111 \rangle$ direction. This was expected since, for this direction, the curves for A and $2B$ for the large and small clusters in Figs. 10 and 12 are very close to each other. For the perpendicular direction, however, there is about 10% difference in the vibrational averages for both A and $2B$, a consequence of the corresponding differences in the curves A and $2B$ in Figs. 11 and 13 for this direction. The differences in the result for the net vibrationally averaged values of A, $2B$, $A_{\parallel}$, and $A_{\perp}$ for the small and large clusters thus originate mainly from the differences in the vibrational averages in the direction perpendicular to $\langle 111 \rangle$. It is encouraging to note from Table IV that these differences are always less than 15%. A comparison of the bond-centered values and the net-averaged values of $A_{\parallel}$ and $A_{\perp}$ in Table IV demonstrates the importance of vibrational averaging for this center, especially for $A_{\parallel}$, where the sign changes after vibrational averaging is carried out. In comparing with experiment, one notices that the net-average value of $A_{\parallel}$ is only about a fourth of experiment while that of $A_{\perp}$ is more than twice the experimental value. A more serious difference between theory and experiment is the relative sign of $A_{\parallel}$ and $A_{\perp}$ which comes out positive from theory in contrast to the negative value found experimentally.[14]

We shall next describe the results we have obtained for the hyperfine properties associated with the relaxed-bond-centered model in silicon. A full-fledged investigation of the hyperfine constants including vibrational averaging as just described for diamond would be rather time consuming for the 27-atom cluster in the case of silicon, due to the much larger number of orbitals involved. However, as we have just seen (Table IV) the values of the muon hyperfine constants in diamond obtained using the small and large clusters did not differ by more than 15%. It appears then that if one is interested in accuracy of this order, it is acceptable in the case of silicon to work with the 9-atom cluster shown in Fig. 2(a). In order to test this point, we have compared the hyperfine properties at the bond center for silicon using both 9- and 27-atom clusters in Figs. 2(a) and 2(b). The displacement of two nearest silicon neighbors Si(1) and Si(2) of the muon in Figs. 2(a) and 2(b) were chosen from the following considerations. Thus, as discussed earlier from the investigations on diamond[47,49] the C(1)-μ^+ and C(2)-μ^+ distances were found to be close to the usual C—H bond distance in organic molecules. Secondly, a recent lattice relaxation[48] calculation for muonium in silicon by the UHF cluster procedure including lattice relaxation effects has shown that the muon occupies an unsymmetric position with the Si-μ^+ distance to the nearer silicon Si(1) being 1.44 Å, close to the usual Si—H bond distance of 1.48 Å in molecular systems. Thirdly, a cluster calculation[50] using the approximate PRDDO method has found a symmetric relaxation of the two nearest silicon atoms, Si(1) and Si(2) with the muon at bond center, the Si(1)-μ^+ and Si(2)-μ^+ distances being both about 1.58 Å, somewhat larger than the usual Si—H bond distance. For our investigations on hyperfine properties, we have chosen the Si(1) and Si(2) atoms to move symmetrically to have the Si(1)-μ^+ and Si(2)-μ^+ distances both equal to the usual Si—H bond distance of 1.48 Å. This choice of the Si-μ^+ distance is a little larger than that found for the nearest Si atom in the UHF investigation and somewhat smaller than that in the PRDDO investigation.[50] We have used this choice of the Si-μ^+ distance so as to be able to test the hyperfine properties for the bond-centered model in the series diamond, silicon, and germanium all with the uniform convention that the neighboring host atoms relax to make their distance from the muon equal to the usual C-H, Si-H, and Ge-H distances in molecular systems. We have also examined the effect of an expansion in the Si-μ^+ distance beyond this choice and studied hyperfine properties for the unsymmetric model found with the UHF investigations.[48] The results from these latter investigations will be described later in this section. We shall consider first our results with the symmetric model.

For this model for silicon, the PEC's and the curves representing variations of A and $2B$ with muon positions along the $\langle 111 \rangle$ axis and perpendicular directions are presented for the 9-atom cluster in Figs. 14 and 15 respectively. Their broad features are very similar to those found for the corresponding curves for diamond in Figs. 8–13. In Table III, we have listed the values of A, $2B$, $A_{\parallel}$, and $A_{\perp}$ at the bond center, the values of these parameters after averaging over vibrational motions of the muon along the $\langle 111 \rangle$ axis and the direction perpendicular to it, as well as the net-average values obtained using Eqs. (10)–(13). The experimental results[13] are listed in the last row for comparison. Since the absolute signs of $A_{\parallel}$ and $A_{\perp}$ are not known we have listed under experimental values those of A and $2B$ for the two possible

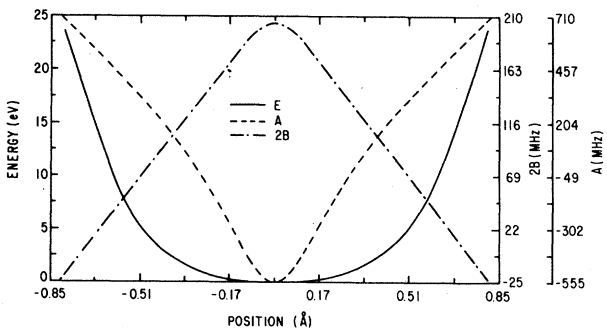

FIG. 14. Potential-energy curve and curves representing variations of muon hyperfine constants A and $2B$ with muon positions along $\langle 111 \rangle$ axis for the BC model in silicon.

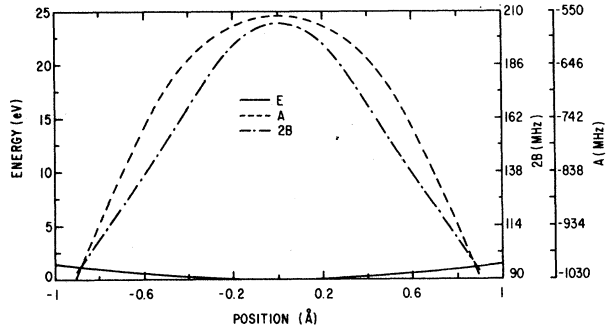

FIG. 15. Potential-energy curve and curves representing variations of muon hyperfine constants A and $2B$ with muon positions along the direction perpendicular to the $\langle 111 \rangle$ axis for the BC model in silicon.

choices of either $A_{\parallel}$ and $A_{\perp}$ both positive or both negative, their ratio being known[13] experimentally to be positive. Almost all of the results in Table V refer to the small or 9-atom cluster in Fig. 2(a). The 27-atom cluster was used, as mentioned earlier, only for the bond-centered location of the muon to test the convergence with respect to cluster size. From the results in Table V, one first notices from the entries under bond-centered values that the results for the 9- and 27-atom clusters are quite close to each other, indicating good convergence with respect to the cluster size. Secondly, vibrational effects are again seen to be quite significant, as in the case of diamond. On comparing the net-average theoretical values of $A_{\parallel}$ and $A_{\perp}$ with experiment,[13] one notices that in contrast to the case of diamond, the relative signs now agree. The magnitudes of the theoretical results are, however, very substantially larger compared to the observed values, by factors of about 12 and 5 for $A_{\parallel}$ and $A_{\perp}$, respectively. Further, from Tables IV and V, the trend in the magnitude of $A_{\parallel}$ in going from diamond to silicon is found to be opposite of experiment,[13,14] while for $A_{\perp}$ the trend is the same as experiment.[13,14] However, in the latter case, the reduction in magnitude is much less, only about a factor of 1.5 from diamond to silicon as compared to the experimental[13,14] ratio of 4.3.

Before passing on to our results for the relaxed BC model in germanium, we would like to point out that we have also evaluated the muon hyperfine constants A, $2B$, $A_{\parallel}$, and $A_{\perp}$ for the somewhat larger bond distance Si(1)-μ^+ [and Si(2)-μ^+] found in the PRDDO investigation.[50] Our results for these parameters in MHz are, respectively, -652.6, 174.0, -478.6, and -739.6. The values of $A_{\parallel}$ and $A_{\perp}$ are seen to be larger than those for the bond-centered position corresponding to Si(1)-μ^+ distance of 1.48 Å listed in Table V. Thus, with the larger bond distance of 1.58 Å, there is a tendency to further increase the substantial difference that already exists between theory and experiment (Table V) for $A_{\parallel}$ and $A_{\perp}$ for the bond distance of 1.48 Å. In view of this, we have not carried out the extensive investigations needed to obtain vibrationally averaged results for the bond distance of 1.58 Å.

Our investigation of hyperfine properties of the relaxed BC model for Mu* in germanium was also carried out using only the 9-atom cluster in Fig. 2(a). In keeping with the model adopted for diamond and silicon, the two nearest-neighbor germanium atoms were displaced from their perfect lattice positions such that the Ge(1)-μ^+ and Ge(2)-μ^+ distances were equal to the usual Ge—H bond length of 1.52 Å. The saturator hydrogen atoms were also placed at a distance of 1.52 Å from the undisplaced position of the Ge(1) and Ge(2). As in the case of silicon, due to the very large number of orbitals and basis functions involved, it was again prohibitively difficult in terms of the computer time involved to carry out UHF cluster investigations for the 27-atom cluster [Fig. 2(b)].

TABLE V. Calculated values of muon hyperfine constants A, $2B$, $A_{\parallel}$, and $A_{\perp}$ in MHz for anomalous muonium in silicon for the bond-centered model.

	Cluster	A	$2B$	$A_{\parallel}$	$A_{\perp}$
Bond-centered value	Small	−556.4	204.5	−351.9	−658.7
	Big	−556.2	192.3	−363.9	−652.3
Average along $\langle 111 \rangle$	Small	−396.2	183.7	−212.5	−488.0
Average along $\langle 111 \rangle_{\perp}$[a]	Small	−583.4	192.1	−391.3	−679.5
Net-average value	Small	−450.2	158.8	−291.4	−529.6
Experimental values[b]		−66.9	50.1	−16.8	−92.0
		66.9	−50.1	16.8	92.0

[a] $\langle 111 \rangle_{\perp}$ denotes direction perpendicular to $\langle 111 \rangle$.

[b] Experimentally (Ref. 13) only the magnitudes of $A_{\parallel}$ and $A_{\perp}$ are known and their ratio has been determined to be positive.

The PEC's and the curves for A and $2B$ as functions of muon position along the ⟨111⟩ direction and in the perpendicular direction are presented in Figs. 16 and 17. The features of these curves are very similar to the corresponding curves for silicon and diamond already discussed.

In Table VI, we have listed for germanium, in the same format as in Tables IV and V for diamond and silicon, the values of A, $2B$, $A_{\parallel}$, and $A_{\perp}$ at the bond center, the values corresponding to averages along ⟨111⟩ axis and the directions perpendicular to it as well as the net average values obtained using Eqs. (10)–(13). For comparison, the experimental results are listed in the last row for the two possible choices of signs of $A_{\parallel}$ and $A_{\perp}$ as in the case of silicon, their relative sign being positive as found experimentally.[13]

From the results in Table VI, it can be seen that the influence of the vibrational averaging effect is again rather significant. The calculated signs of $A_{\parallel}$ and $A_{\perp}$ are found to be the same, in agreement with experimental observation.[13] However, the magnitudes of the net-averaged values are much too high compared to experiment,[13] by factors of 18 and 5 for $A_{\parallel}$ and $A_{\perp}$, respectively. The trend in the magnitudes of $A_{\parallel}$ and $A_{\perp}$ as compared to silicon is found to agree with experiment,[13] but the trend with respect to diamond is opposite compared to experiment.[13,14]

Using the UHF wave functions obtained from our investigations on the bond-centered model, we have also studied the superhyperfine interaction parameters of the nearest-neighbor ^{13}C, ^{29}Si, and ^{73}Ge nuclei using Eqs. (4) which are presented in Table VII. For all three systems, the results are presented for the case of the muon located at the bond center. The vibrational motion of the muon would, in principle, be expected to influence these results. However, since we are now looking at the hyperfine constants for nuclei which are virtually stationary, vibrational effects are expected to be less pronounced than in the case of the muon hyperfine parameters, where the spin density is evaluated at the site of the vibrating nucleus (muon).

It should also be mentioned that for diamond and silicon we have studied the superhyperfine-interaction parameters both in 9- and 27-atom clusters. But in the case of germanium, only the 9-atom cluster has been studied, therefore no results are available for the bigger cluster.

In the 9-atom cluster, the nearest neighbors of the host atoms, for which superhyperfine interaction has been studied, are replaced by hydrogen atoms, whereas in the 27-atom cluster these neighboring host atoms are included. Consequently, in making comparison with experiment, it is preferable to use the superhyperfine-interaction constants from the larger cluster.

The only experimental result available for superhyperfine-interaction parameters is from a recent level crossing resonance experiment for Mu* in silicon.[19] The analysis of the LCR data on the basis of the bond-centered model yields the values $A_{\parallel}^{n}(^{29}\mathrm{Si}) = -137.5$ MHz, $A_{\perp}^{n}(^{29}\mathrm{Si}) = -74$ MHz. On comparing these values with the corresponding values in Table VII, for the 27-atom cluster, the theoretical values are again found, as in the case of muon hyperfine interactions, to be larger than experiment[19] although the disagreement is much less severe. We shall remark in Sec. VI on various aspects of the LCR measurements[19] that provided the superhyperfine parameters for silicon.

As mentioned earlier, a recent UHF cluster investigation[48] including lattice relaxation of nearest neighbors of muon in silicon has found an asymmetric location for the muon in the intrabond region (hereafter it will be referred to as IB model) in contrast to the bond-centered location found in the earlier PRDDO cluster calculations[50] and recent supercell calculations.[51] The off-center location has also been supported by a recent cluster investigation[52] on hydrogen in silicon using the approximate MNDO procedure. We have therefore analyzed the muon as well as the neighboring ^{29}Si hyperfine parameters for the IB model using both the 9-atom cluster shown in Fig. 2(a) and the 27-atom cluster shown in Fig. 2(b). The small cluster was used to calculate the PEC for muon which was utilized in carrying out the vibrational averaging of the muon hyperfine parameters following the same procedure as for the BC model. The convergence of the results with cluster size was tested by repeating the calculation of the hyperfine constants using the 27-atom cluster at the position of the muon corresponding to the energy

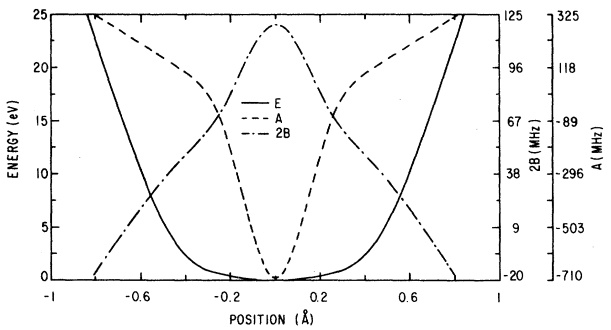

FIG. 16. Potential-energy curve and curves representing variations of muon hyperfine constants A and $2B$ with muon positions along ⟨111⟩ axis for the BC model in germanium.

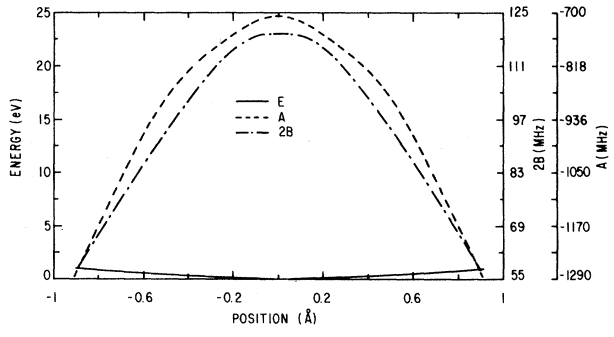

FIG. 17. Potential-energy curve and curves representing variations of muon hyperfine constants A and $2B$ with muon positions along the direction perpendicular to the ⟨111⟩ axis for the BC model in germanium.

TABLE VI. Calculated values[a] of muon hyperfine constants A, $2B$, $A_{\parallel}$, and $A_{\perp}$ in MHz for anomalous muonium in germanium for the bond-centered model.

	A	$2B$	$A_{\parallel}$	$A_{\perp}$
Bond-centered value	−704.4	119.9	−584.5	−764.3
Average along ⟨111⟩	−480.7	102.6	−378.1	−532.0
Average along $\langle 111\rangle_{\perp}$[b]	−760.9	113.5	−647.4	−817.6
Net-average value	−593.7	89.8	−503.9	−638.6
Experimental values[c]	−96.1 96.1	69.2 −69.2	−26.8 26.8	−130.7 130.7

[a]All results are for the small cluster in Fig. 2(a).
[b]$\langle 111\rangle_{\perp}$ denotes direction perpendicular to ⟨111⟩.
[c]Experimentally (Ref. 13) only the absolute values of hyperfine tensor components are known and the ratio between parallel and perpendicular components are found to be positive.

minimum for the small cluster. The nearest-neighbor silicon atoms Si(1) and Si(2) in Figs. 2(a) and 2(b) were displaced from their equilibrium positions by amounts of 0.38 and 0.44 Å, respectively, away from each other, as found from the recent UHF cluster calculations[48] including lattice relaxation. The saturator hydrogen atoms were placed at a distance of 1.48 Å from the unrelaxed position of the silicon atoms in the perfect lattice as in our work on the relaxed BC model. The geometry used for the 27-atom cluster is exactly same as that obtained in the recent UHF cluster calculation.[48]

An absolute minimum in the PEC was found at a distance of 1.44 Å from the Si(1). In Table VIII(a) we have listed the values of A, $2B$, $A_{\parallel}$, and $A_{\perp}$ for muon at the minimum position in PEC, their average values for muon vibration along different directions and their net average values. The agreement between the values of these hyperfine parameters for small and large clusters are again very close to each other. As in the case of the results for the relaxed BC model in Si listed in Table V, the relative sign of the net-average values of $A_{\parallel}$ and $A_{\perp}$ agrees with experiment,[13] but their magnitudes are again overestimated by substantially large factors, namely 19 and 5, respectively. We have also evaluated the ^{29}Si hyperfine parameters for both the neighboring silicon atoms of muon when the latter is at the position on the ⟨111⟩ axis corresponding to the absolute minimum in the PEC. Unlike the relaxed BC model, we now have two inequivalent silicon nuclei. The values obtained for the ^{29}Si hyperfine parameters from our UHF cluster calculations are listed in Table VIII(b). The values for the two nuclei are significantly different from each other as expected for the IB model, the values of $A_{\parallel}^{n}$ and $A_{\perp}^{n}$ are factors between 2 and 3 larger than the single set of values derived from recent LCR measurements[19] making use of the BC model.

Before passing on to the final section presenting concluding remarks, it is important to summarize the main features of the results of comparison between the theoretical predictions of the relaxed BC model for the hyperfine parameters through UHF cluster calculations and experimental results.[13,14,19]

TABLE VII. Superhyperfine constants in MHz for ^{13}C, ^{29}Si, and ^{73}Ge obtained from theoretical investigations for the bond-centered model for Mu* and experimental values for silicon.

		Theory				Experiment[a]	
Semiconductor	Cluster	A	$2B$	$A_{\parallel}$	$A_{\perp}$	$A_{\parallel}$	$A_{\perp}$
Diamond	Small	438.9	80.7	519.6	398.5		
	Big	301.7	95.3	396.9	254.1		
Silicon	Small	−278.4	−107.3	−385.7	−224.7	−137.5	−74.0
	Big	−184.7	−110.0	−294.7	−129.7		
Germanium	Small	−66.4	2.9	−63.5	−67.9		

[a]Taken from Ref. 19.

TABLE VIII. (a) Muon hyperfine constants in MHz for anomalous muonium in silicon for the intrabond model. (b) ^{29}Si superhyperfine parameters in MHz for anomalous muonium in silicon for the intrabond model.

(a)

	Cluster	A	$2B$	$A_{\parallel}$	$A_{\perp}$
At the minimum position of PEC	Small	−367.5	140.4	−227.1	−437.7
	Big	−396.2	158.4	−237.8	−475.4
Average along ⟨111⟩	Small	−448.3	148.8	−299.5	−522.7
Average along $\langle 111\rangle_{\perp}$	Small	−383.2	132.5	−250.7	−449.4
Net-average value	Small	−479.7	133.0	−346.7	−546.3
Experimental values[a]		−66.9 66.9	50.1 −50.1	−16.8 16.8	−92.0 92.0

(b)

Cluster	Neighbor[b]	A	$2B$	$A_{\parallel}^{n}$	$A_{\parallel}^{n}$
Small	First	−149.2	−60.5	−209.7	−119.0
Big	First	−173.4	−65.6	−239.0	−140.6
Small	Second	−216.2	−140.8	−357.0	−145.8
Big	Second	−230.3	−139.0	−369.3	−160.8
Experiment[c]				−137.5	−74.0

[a]Experimentally (Ref. 13) only the absolute values of $A_{\parallel}$ and $A_{\perp}$ are known and their ratio has been determined to be positive.
[b]The first and second neighbors in this table refer to the two closest silicon atoms nearer and further, respectively, from the muon in the IB model.
[c]Taken from Ref. 19.

(a) The relaxed BC model, with the sole exception of $A_{\parallel}$ in the case of diamond, seriously overestimates the magnitudes of the hyperfine constants with respect to experiment[13,14,19] by factors in the range 2–20. It has been suggested in the literature[49] that incorporation of many-body effects could reduce the hyperfine constants, bringing them closer to experiment. However, many-body perturbation theoretical calculations[41,63] on CH and OH free radicals (which are pertinent to the BC model since the latter involves C—H, Si—H, Ge—H type bonds with the muonium) suggest that many-body effects actually increase the hyperfine constant above the one-electron value. Additionally, their effects are much too small to bridge the large gaps with experiment found for the relaxed BC model.

(b) The results of the relaxed BC model do explain the oblate nature of muon hyperfine tensor found experimentally.[13,14]

(c) The relaxed BC model cannot explain the observed[13,14] relative sign of $A_{\parallel}$ and $A_{\perp}$ in diamond, although it does explain the observed relative signs[13,14] in silicon and germanium.

(d) The relaxed BC model is not successful in explaining the observed trend in the strength of the muon hyperfine tensor in going from diamond to germanium, as obtained from μSR hyperfine data.[13,14]

(e) The relaxed BC model predicts the correct signs of the ^{29}Si superhyperfine tensor components derived from LCR data[19] but overestimates their magnitudes by factors close to 2.

(f) The question of whether the location of the muon in the intrabond region is symmetric (BC) or nonsymmetric (IB) is not yet certain from energy considerations from the various theoretical investigations[47–52] that have been carried out. Both the relaxed BC and IB models predict substantially higher values for the muon hyperfine parameters compared to experiment.[13,14]

VI. CONCLUDING REMARKS

The results of our investigation on the various models that have been proposed for anomalous muonium have been described in Secs. IV and V. From these results it is quite clear that, as mentioned earlier, there are presently two viable models for Mu*, namely the BC model and the VA model. Both of these models have provided[47–52] absolute minima in the associated potential-energy curves

indicating stable configurations for the μ^+e^- complex. Turning first to the BC model, this model has received its strongest support from the results of LCR measurements. Thus, the LCR measurement on silicon[19] indicates that the ratio of the intensities of the main lines and satellites associated with the ^{29}Si is close to what one would expect with two equivalent silicon atoms on either side of the muon and the relative abundance of ^{28}Si and ^{29}Si nuclei. The premise of equivalent silicon atoms on either side of the muon could have some difficulty when one considers the conclusion from one of the recent theoretical investigations which suggest that the minimum in the potential energy curve for the muon occurs at a point much closer to one of the two adjacent atoms, for instance, B in Figs. 2(a) and 2(b), than to the other, namely E. However, there will be an equivalent complementary minimum closer to E than to B, leading to a double-well potential in these investigations. A fast tunneling between these two minima could still justify the consideration of equivalence between silicon atoms B and E. The magnitudes of the superhyperfine parameters for ^{29}Si are seen from Table VIII(b) (averages for the two inequivalent ^{29}Si atoms to be taken in this case) to be about a factor of 3 larger than those derived from LCR results. This is, however, not too worrisome because these ^{29}Si superhyperfine constants are expected to depend sensitively on lattice relaxation involving movement of their other silicon neighbors which has not been included in the calculation. Further support for the BC model in silicon has been provided through the interpretation[18] of the LCR data in GaAs as arising out of only two inequivalent nuclei, ^{69,71}Ga and ^{75}As adjacent to the muon.

As explained earlier, it was this strong support in the literature for the BC model from the LCR data[18,19] that led us to examine the muon hyperfine properties for this model. The analysis of the results in Tables IV–VI indicates that the BC model does explain the oblateness of the observed hyperfine tensors in all three systems, diamond, silicon, and germanium, and the negative sign for $A_\perp$ for diamond. However, with this model one is not able to explain the trend in the strengths of the hyperfine interactions over the series, diamond, silicon, and germanium, and the reversal sign of $A_\parallel/A_\perp$ in going from diamond to the two other elemental semiconductors. Additionally, this model leads to a very substantial overestimation of the strengths of the hyperfine interactions, by as much as a factor of 18 in the case of $A_\parallel$ in germanium. The results with the intrabond model in Table VII have the same features in this respect as the BC model. It has been suggested[49] in the literature that perhaps the many-body effect could reduce the large hyperfine interactions obtained through Hartree-Fock cluster theory as applied to Mu*. However, many-body calculations of hyperfine properties of molecular systems[41,55] indicate not only that these effects cannot lead to the very large corrections needed to make the predicted results in Tables IV–VI to agree with experiment, but that these effects lead to increases in the strengths of hyperfine interactions rather than decreases.

Thus, one has the intriguing situation that while the BC model appears to be successful in explaining the results of LCR experiments, it has some serious difficulties in explaining the features and magnitudes of the observed muon hyperfine constants in the three elemental semiconductors. One thus needs a modification of this model which will retain its attractive feature of agreement with the results of LCR measurements while attempting to narrow the disagreement with muon hyperfine data.

Turning next to the VA model, it has been shown in the present work to have the ability to explain all the observed features of the muon hyperfine data.[13,14] Thus, it has explained very well (Table II) the trend in the strength of the hyperfine interactions in diamond through germanium, the oblateness of the hyperfine tensor, the relative sign of $A_\parallel$ and $A_\perp$, and the absolute sign of $A_\perp$ for diamond. Additionally, it has provided satisfactory agreement with experiment for the absolute strengths of the hyperfine parameters in silicon and germanium. In diamond, the theoretical values are somewhat underestimated compared to experiment. In this context the need for studying the influence of lattice relaxation and many-body effects which require additional computational efforts has been pointed out in the discussion in Sec. IV.

While the VA model thus appears to be more successful in explaining available muonium hyperfine data than the BC model, the latter has the advantage of being able to provide a more direct explanation of the nature of available LCR data. It should, however, be pointed out that the VA model cannot be considered as completely ruled out based on the interpretation of LCR measurements. This is because, unlike the BC model where only two nearest-neighbor host nuclei with a significant super-hyperfine constant are involved and so the analysis of LCR data is straightforward, in the case of the VA model due to the presence of a larger number of nearest-neighbor nuclei, the analysis of the satellite spectra due to the superhyperfine interactions of the latter nuclei is more complex. It is hoped that the results we have presented for the superhyperfine constants for the VA model in Table III will be utilized in the future to compare the predicted LCR pattern with observed ones to test this model, admittedly a rather complex task.

A number of experimental observations[13,14,59–63] which provide indirect support for the VA model have been already discussed in Sec. V. The main question that remains to be answered for the VA model is the mechanism for the trapping process of the μ^+e^- pair at the vacancy, namely whether this pair gets trapped at existing vacancies or whether the muon produces the vacancy, the vacancy-muon environment trapping an unpaired electron. The inability of preformed vacancies in electron-irradiated samples[13,20] to increase the initial Mu* amplitude could be thought of as arguing against the muonium getting trapped near existing vacancies. But the second mechanism could still be a source for formation of the Mu* center. Support for this second mechanism for formation of Mu* in the context of the VA model is available from Mu to Mu* conversion studies[13,16] in diamond. These studies suggest that the conversion process involves a single over-barrier jump of the muon. This feature would be difficult to explain if the Mu* center in-

volved μ^+e^- complex searching for a vacancy to get trapped at. But if the vacancy was formed by the muon itself, the explanation of a single barrier jump associated with the Mu to Mu* conversion would be more compatible with the VA model. Theoretical investigations addressed to answering these questions would require dynamical studies and are expected to be rather complicated. We hope the results of the present analysis will stimulate such investigations in the future using advanced computing facilities.

In conclusion, it appears that in many respects, the question of the appropriate model for explaining all the observed features[13,14,16,17] of the Mu* center is still an open one. What is needed is a model that combines the features of the BC model of two nearest-neighbor host nuclei which allow one to explain the nature of the observed LCR data and does not raise difficult questions of formation of the Mu* center, with some of the features of the VA model including weaker confinement of the unpaired spin density near the muon which allows one to explain the observed muon data. It is hoped that the results of the present investigation will stimulate further efforts along these lines.

---

*Present address: GTE Electrical Products, 100 Endicott Street, Danvers, MA 01923.

[1]J. H. Brewer, K. M. Crowe, F. N. Gygax, and A. Schenck, in *Muon Physics,* edited by V. W. Hughes and C. S. Wu (Academic, New York, 1975), Vol. III, p. 3; A. Schenck, *Muon Spin Rotation Spectroscopy: Principles and Applications in Solid State Physics* (Hilger, Bristol, 1985); B. D. Patterson, Rev. Mod. Phys. **60**, 69 (1988).

[2]E. Holzschuh, W. Kündig, P. F. Meier, B. D. Patterson, J. P. F. Sellschop, M. C. Stemmet, and H. Appel, Phys. Rev. A **25**, 1272 (1982); J. H. Brewer, K. M. Crowe, F. N. Gygax, R. F. Johnson, B. D. Patterson, D. G. Fleming, and A. Schenck, Phys. Rev. Lett. **31**, 143 (1973); E. Holzschuh, H. Graf, E. Recknagel, A. Weidinger, T. Wichert, and P. F. Meier, Phys. Rev. B **20**, 4391 (1979); B. D. Patterson, A. Hinterman, W. Kündig, P. F. Meier, F. Waldner, H. Graf, E. Recknagel, A. Weidinger, and T. Wichert, Phys. Rev. Lett. **40**, 1347 (1978).

[3]R. F. Kiefl, J. W. Schneider, H. Keller, W. Kündig, W. Odermatt, B. D. Patterson, K. W. Blazey, T. L. Estle, and S. L. Rudaz, Phys. Rev. B **32**, 530 (1985).

[4]R. F. Kiefl, M. Celio, T. L. Estle, G. M. Luke, J. H. Brewer, D. R. Noakes, E. J. Ansaldo, and K. Nishiyama, Phys. Rev. Lett. **58**, 1780 (1987); R. F. Kiefl, M. Celio, T. L. Estle, S. R. Kreitzman, G. M. Luke, T. M. Riseman, and E. J. Ansaldo, *ibid.* **60**, 224 (1988).

[5]N. Sahoo, S. K. Mishra, K. C. Mishra, A. Coker, T. P. Das, C. K. Mitra, L. C. Snyder, and A. Glodeanu, Phys. Rev. Lett. **50**, 913 (1983); Hyperfine Interact. **17-19**, 525 (1984); N. Sahoo, K. C. Mishra, and T. P. Das, *ibid.* **32**, 601 (1986); H. Katayama-Yoshida and K. Shindo, Phys. Rev. Lett. **51**, 207 (1983); W. E. Pickett, M. L. Cohen, and C. Kittel, Phys. Rev. B **20**, 5050 (1979); M. Manninen and P. F. Meier, *ibid.* **26**, 6690 (1982); S. Estreicher, A. K. Ray, J. L. Fry, and D. S. Marynick, Phys. Rev. Lett. **55**, 1976 (1985), Phys. Rev. B **34**, 6071 (1986); T. A. Claxton, A. Evans, and M. C. R. Symons, J. Chem. Soc. Faraday Trans. 2 **82**, 2031 (1986); S. Estreicher, Phys. Rev. B **36**, 9122 (1987).

[6]T. L. Estle, Hyperfine Interact. **8**, 365 (1978), **17-19**, 585 (1984); M. C. R. Symons, *ibid.* **17-19**, 771 (1984).

[7]N. Sahoo, S. K. Mishra, K. C. Mishra, A. Coker, T. P. Das, C. K. Mitra, L. C. Snyder, and A. Glodeanu, Hyperfine Interact. **17-19**, 525 (1984).

[8]N. Sahoo, K. C. Mishra, and T. P. Das, Phys. Rev. Lett. **55**, 1506 (1985).

[9]N. Sahoo, Ph.D. thesis, State University of New York at Albany, 1986 (unpublished).

[10]N. Sahoo, K. C. Mishra, T. P. Das, and P. C. Schmidt, Hyperfine Interact. **32**, 619 (1987).

[11]N. Sahoo, K. C. Mishra, and T. P. Das, Hyperfine Interact. **32**, 779 (1987).

[12]T. A. Claxton, A. Evans, and M. C. R. Symons, J. Chem. Soc. Faraday Trans. 2 **82**, 2031 (1986); T. L. Estle, S. Estreicher, and D. S. Marynick, Phys. Rev. Lett. **58**, 1547 (1987).

[13]For a review of experimental results, see, B. D. Patterson, Rev. Mod. Phys. **60**, 69 (1988).

[14]E. Holzschuh, W. Kündig, P. F. Meier, B. D. Patterson, J. P. F. Sellschop, M. C. Stemmet, and H. Appel, Phys. Rev. A **25**, 1272 (1982), and references therein.

[15]T. L. Estle, Hyperfine Interact. **17-19**, 585 (1984).

[16]B. D. Patterson, E. Holzschuh, W. Kündig, P. F. Meier, W. Odermatt, J. P. F. Sellschop, and M. C. Stemmet, Hyperfine Interact. **17-19**, 605 (1984); W. Odermatt, Hp. Baumeler, H. Keller, W. Kündig, B. D. Patterson, J. W. Schneider, J. P. F. Sellschop, M. C. Stemmet, S. Connell, and D. P. Spencer, *ibid.* **32**, 583 (1986); W. Odermat, Hp. Baumeler, H. Keller, W. Kundig, B. D. Patterson, J. W. Schneider, J. P. F. Sellschop, M. C. Stemmet, S. Connell, and D. P. Spencer, Phys. Rev. B **38**, 4388 (1988).

[17]B. D. Patterson, A. Bosshard, U. Straumann, P. Truol, A. Wuest, and Th. Wichert, Phys. Rev. Lett. **52**, 938 (1984); Hyperfine Interact. **17-19**, 695 (1984).

[18]R. F. Kiefl *et al.*, Phys. Rev. Lett. **58**, 1780 (1987).

[19]R. F. Kiefl *et al.*, Phys. Rev. Lett. **60**, 224 (1988).

[20]E. Albert, A. Möslang, E. Recknagel, and A. Weidinger, Hyperfine Interact. **17-19**, 611 (1984); E. Albert, S. Barth, A. Moslang, E. Recknagel, A. Weidinger, and P. Moser, Appl. Phys. Lett. **46**, 759 (1985).

[21]For a review see, E. A. Colbourn and J. Kendrick, in *Computer Simulation of Solids,* edited by C. R. A. Catlow and W. C. Mackrodt (Springer-Verlag, New York, 1982), p. 67; A. M. Stoneham, *ibid.*, p. 207.

[22]See, for instance, P. S. Bagus, C. R. Brundle, T. J. Chuang, and K. Wandelt, Phys. Rev. Lett. **39**, 1229 (1977); G. T. Surratt and A. B. Kunz, Solid State Commun. **23**, 555 (1977); S. Nagel, J. Phys. C **18**, 3673 (1985); P. C. Kelires and T. P. Das, Hyperfine Interact. **34**, 285 (1987); P. C. Kelires, K. C. Mishra, and T. P. Das, *ibid.* **34**, 289 (1987); J. Q. Broughton and P. S. Bagus, Phys. Rev. B **36**, 2813 (1987).

[23]See, for instance, R. P. Messmer and G. D. Watkins, Phys. Rev. Lett. **25**, 656 (1970); N. Sahoo *et al.*, *ibid.* **50**, 913 (1983); G. T. Suratt and W. A. Goddard III, Phys. Rev. B **18**, 2831 (1978); J. C. Malvido and J. L. Whitten, *ibid.* **26**, 4458 (1982).

[24]See, for instance, J. Isoya, J. A. Weil, and L. E. Halliburton, J. Chem. Phys. **74**, 5436 (1981); T. M. Wilson, J. A. Weil, and P.

S. Rao, Phys. Rev. B **34**, 6053 (1986).
[25]See, for instance, B. N. Dev, K. C. Mishra, W. M. Gibson, and T. P. Das, Phys. Rev. B **29**, 1101 (1984); M. Seel and P. S. Bagus, *ibid.* **8**, 2023 (1983); A. D. Zdetsis and A. B. Kunz, *ibid.* **32**, 6358 (1985); J. C. Malvido and J. L. Whitten, *ibid.* **26**, 4458 (1982); I. P. Batra, P. S. Bagus, and K. Herman, Phys. Rev. Lett. **52**, 384 (1984).
[26]See, for instance, F. P. Larkins, J. Phys. C **4**, 3065 (1971); C. A. Swarts, W. A. Goddard III, and T. C. McGill, J. Vac. Sci. Technol. **19**, 551 (1981), A. C. Kenton and W. M. Ribarsky, Phys. Rev. B **23**, 2897 (1981); N. Sahoo *et al.*, Phys. Rev. Lett. **50**, 913 (1983); B. N. Dev *et al.*, Phys. Rev. B **29**, 1101 (1984).
[27]J. A. Pople and R. K. Nesbet, J. Chem. Phys. **22**, 571 (1954); R. E. Watson and A. J. Freeman, in *Hyperfine Interaction,* edited by A. J. Freeman and R. B. Frankel (Academic, New York, 1967).
[28]C. C. J. Roothaan, Rev. Mod. Phys. **23**, 69 (1951).
[29]S. F. Boys, Proc. R. Soc. London Ser. A **200**, 542 (1950).
[30]R. McWeeny and B. T. Sutcliffe, *Methods of Molecular Quantum Mechanics* (Academic, New York, 1969), p. 213.
[31]W. J. Hehre, R. F. Stewart, and J. A. Pople, J. Chem. Phys. **51**, 2657 (1969); W. J. Hehre, R. Ditchfield, R. F. Stewart, and J. A. Pople, *ibid.* **52**, 2769 (1970); W. J. Pietro, B. A. Levi, W. J. Hehre, and R. F. Stewart, Inorg. Chem. **19**, 2225 (1980).
[32]J. S. Binkley, J. A. Pople, and W. J. Hehre, J. Am. Chem. Soc. **102**, 939 (1980); M. S. Gordon, J. S. Binkley, J. A. Pople, and W. J. Hehre, *ibid.* **104**, 2797 (1982); K. D. Dobbs and W. J. Hehre, J. Comput. Chem. **7**, 359 (1986).
[33]See, for instance, N. Sahoo *et al.*, Phys. Rev. Lett. **50**, 913 (1983); B. N. Dev *et al.*, Phys. Rev. B **29**, 1101 (1984); B. K. Rao, P. Jena, and M. Manninen, Phys. Rev. Lett. **53**, 2300 (1984); T. M. Wilson, J. A. Weil, and P. S. Rao, Phys. Rev. B **34**, 6053 (1986); S. M. Mohapatra, B. N. Dev, K. C. Mishra, N. Sahoo, W. M. Gibson, and T. P. Das, Phys. Rev. B **38**, 12 556 (1988).
[34]J. S. Binkley, R. A. Whiteside, R. Krishnan, R. Seeger, D. J. DeFrees, H. B. Schlegel, and J. A. Pople, GAUSSIAN-80: An *ab initio* Molecular Orbital Program, Quantum Chemistry Program Exchange, Indiana University, Bloomington, Indiana, Program No. 437.
[35]M. J. Frisch, J. S. Binkley, H. B. Schlegel, K. Raghavachari, C. F. Melius, R. L. Martin, J. J. P. Stewart, F. W. Bobrowicz, C. M. Rohlfing, L. R. Kahn, D. J. Defrees, R. Seeger, R. A. Whiteside, D. J. Fox, E. M. Fleuder, and J. A. Pople, GAUSSIAN-86, Carnegie-Mellon Quantum Chemistry Publishing Unit, Pittsburgh, Pennsylvania, 1984.
[36]E. B. Wilson, J. C. Decius, and P. C. Cross, *Molecular Vibration* (McGraw-Hill, New York, 1955), Chap. 6.
[37]T. L. Estle, Hyperfine Interact. **8**, 365 (1978).
[38]A. Coker, T. Lee, and T. P. Das (unpublished); A. Coker, T. P. Das, and A. Glodeanu, Bull. Am. Phys. Soc. **25**, 204 (1980).
[39]R. Hoffman, J. Chem. Phys. **39**, 1397 (1963); M. Zerner, M. Gouterman, and H. Kobayashi, Theor. Chim. Acta **6**, 363 (1966); M. F. Rettig, P. S. Han, and T. P. Das, *ibid.* **12**, 178 (1968).
[40]S. T. Picraux and F. L. Vook, Phys. Rev. B **18**, 2066 (1978).
[41]J. E. Rodgers, T. Lee, D. Ikenberry, and T. P. Das, Phys. Rev. A **7**, 51 (1973).
[42]N. Sahoo *et al.*, Phys. Rev. Lett. **50**, 913 (1983).
[43]N. Sahoo, K. C. Mishra, and T. P. Das, Hyperfine Interact. **32**, 601 (1986).
[44]N. Sahoo, K. C. Mishra, and T. P. Das, Phys. Rev. Lett. **57**, 3300 (1986).
[45]J. C. Phillips, *Bonds and Bands in Semiconductors* (Academic, New York, 1973), p. 42.
[46]M. C. R. Symons, Hyperfine Interact. **17-19**, 771 (1984).
[47]T. A. Claxton, A. Evans, and M. C. R. Symons, J. Chem. Soc. Faraday Trans. 2 **82**, 2031 (1986).
[48]A. Amore Bonapasta, A. Lapiccirella, N. Tomassini, and M. Capizzi, Europhys. Lett. **7**, 145 (1988).
[49]T. L. Estle, S. Estreicher, and D. S. Marynick, Hyperfine Interact. **32**, 637 (1986), Phys. Rev. Lett. **58**, 1947 (1987).
[50]S. Estreicher, Phys. Rev. B **36**, 9122 (1987).
[51]Chris G. Van de Walle, Y. Bar-Yam, and S. T. Pantelides, Phys. Rev. Lett. **60**, 2761 (1988).
[52]G. G. DeLeo, M. J. Dorogi, and W. Beall Fowler, Bull. Am. Phys. Soc. **33**, 698 (1988), Phys. Rev. B **38**, 7520 (1988).
[53]A brief report of our results on the BC model was presented at the March meeting of the American Physical Society, 1988, New Orleans, Louisiana [Bull. Am. Phys. Soc. **33**, 567 (1988)].
[54]G. D. Watkins, in *Lattice Defects in Semiconductors 1974,* Institute of Physics Conference Series No. 23, edited by F. A. Huntley (IOP, London, 1975), p. 1; G. A. Baraff, E. O. Kane, and M. Schlüter, Phys. Rev. Lett. **43**, 956 (1979).
[55]H. A. Jahn and E. Teller, Proc. R. Soc. London Ser. A **161**, 220 (1937).
[56]J. Bernholc, N. O. Lipari, and S. T. Pantelidis, Phys. Rev. B **21**, 3545 (1980); G. A. Baraff, E. O. Kane, and M. Schlüter, *ibid.* **21**, 5662 (1980); J. C. Malvido and J. L. Whitten, *ibid.* **26**, 4458 (1982); M. Lanoo, *ibid.* **28**, 2403 (1983).
[57]H. J. Stein, Phys. Rev. Lett. **43**, 1030 (1979).
[58]K. Irmscher, H. Klose, and K. Haas, J. Phys. C **17**, 6317 (1984).
[59]W. Frank, in *Lattice Defects in Semiconductors 1974,* Institute of Physics Conference Series No. 23, edited by F. A. Huntley (IOP, London, 1975), p. 23.
[60]J. C. Bourgoin, P. M. Mooney, and F. Poulin, in *Defects and Radiation Effects in Semiconductors,* Institute of Physics Conference Series No. 59, edited by R. R. Hasiguti (IOP, Bristol, 1981), p. 33.
[61]J. H. N. Loubser and J. A. van Wyk, Rep. Prog. Phys. **41**, 1201 (1978).
[62]R. Poirier, R. Kari, and I. G. Csizmadia, *Handbook of Gaussian Basis Sets* (Elsevier, Amsterdam, 1985), p. 156.
[63]P. Kristiansen and L. Veseth, J. Chem. Phys. **84**, 2711 (1986); **84**, 6336 (1986).